

Lawrence Berkeley National Laboratory

LBL Publications

Title

Gravitational waves from stochastic scalar fluctuations

Permalink

<https://escholarship.org/uc/item/1xz4g152>

Journal

Physical Review D, 109(8)

ISSN

2470-0010

Authors

Ebadi, Reza

Kumar, Soubhik

McCune, Amara

et al.

Publication Date

2024-04-15

DOI

10.1103/physrevd.109.083519

Copyright Information

This work is made available under the terms of a Creative Commons Attribution License, available at <https://creativecommons.org/licenses/by/4.0/>

Peer reviewed

Gravitational Waves from Stochastic Scalar Fluctuations

Reza Ebadi,^{1,2} Soubhik Kumar,^{3,4} Amara McCune,^{3,4,5} Hanwen Tai,⁶ and Lian-Tao Wang^{6,7,8}

¹*Department of Physics, University of Maryland, College Park, MD 20742, USA*

²*Quantum Technology Center, University of Maryland, College Park, MD 20742, USA*

³*Berkeley Center for Theoretical Physics, Department of Physics,
University of California, Berkeley, CA 94720, USA*

⁴*Theoretical Physics Group, Lawrence Berkeley National Laboratory, Berkeley, CA 94720, USA*

⁵*Department of Physics, University of California, Santa Barbara, CA 93106, USA*

⁶*Department of Physics, The University of Chicago, Chicago, IL 60637, USA*

⁷*Enrico Fermi Institute, University of Chicago, Chicago, Illinois 60637, USA*

⁸*Kavli Institute for Cosmological Physics, University of Chicago, Chicago, Illinois 60637, USA*

We present a novel mechanism for gravitational wave generation in the early Universe. Light spectator scalar fields during inflation can acquire a blue-tilted power spectrum due to stochastic effects. We show that this effect can lead to large curvature perturbations at small scales (induced by the spectator field fluctuations) while maintaining the observed, slightly red-tilted curvature perturbations at large cosmological scales (induced by the inflaton fluctuations). Along with other observational signatures, such as enhanced dark matter substructure, large curvature perturbations can induce a stochastic gravitational wave background (SGWB). The predicted strength of SGWB in our scenario, $\Omega_{\text{GWB}} h^2 \simeq 10^{-20} - 10^{-15}$, can be observed with future detectors, operating between 10^{-5} Hz and 10 Hz. We note that, in order to accommodate the newly reported NANOGrav observation, one could consider the same class of spectator models. At the same time, one would need to go beyond the simple benchmark considered here and consider a regime in which a misalignment contribution is also important.

CONTENTS

		4. Recasting integrals for numerical computation	14
I. Introduction	1	5. Useful formula	15
II. Cosmological History and Curvature Perturbation	3	References	16
III. Review of the Stochastic Formalism	4		
A. Langevin and Fokker-Planck Equations	5		
B. Two-point Correlation Function and Power Spectrum	5		
IV. Large Curvature Perturbation from Stochastic Fluctuations	6		
A. Equilibrium Configuration	6		
B. Power Spectrum	7		
V. Gravitational Wave Signature	9		
A. Secondary Gravitational Waves from Scalar Curvature Perturbation	9		
VI. Conclusion	11		
Note Added	11		
Acknowledgment	12		
A. Scalar-induced gravitational waves: technical details	12		
1. Transfer functions	12		
2. Green's function and GW solution	13		
3. Connected and disconnected 4-point correlation function	14		

I. INTRODUCTION

The fluctuations observed in the cosmic microwave background (CMB) and large-scale structure (LSS) have given us valuable information about the primordial Universe. As per the standard Λ CDM cosmology, such fluctuations were generated during a period of cosmic inflation (see [1] for a review). While the microphysical nature of inflation is still unknown, well-motivated single-field slow-roll inflationary models predict an approximately scale-invariant spectrum of primordial fluctuations, consistent with CMB and LSS observations. These observations have enabled precise measurements of the primordial fluctuations between the comoving scales $k \sim 10^{-4} - 1 \text{ Mpc}^{-1}$. However, the properties of primordial density perturbations are comparatively much less constrained for $k \gtrsim \text{Mpc}^{-1}$. In particular, as we will discuss below, the primordial curvature power spectrum Δ_{ζ}^2 can naturally be much larger at such small scales, compared to the value $\Delta_{\zeta}^2 \approx 2 \times 10^{-9}$ observed on CMB scales [2].

Scales corresponding to $k \gtrsim \text{Mpc}^{-1}$ are interesting for several reasons. First, they contain vital information regarding the inflationary dynamics after the CMB-observable modes exit the horizon. In particular, they can reveal important clues as to how inflation could have

ended and the Universe was reheated. An enhanced power spectrum on such scales can also lead to overabundant dark matter (DM) subhalos, motivating novel probes (see [3] for a review). Furthermore, if the enhancement is significant, $\Delta_\zeta^2 \gtrsim 10^{-7}$, the primordial curvature fluctuations can induce a stochastic gravitational wave background (SGWB) within the range of future gravitational wave detectors [4]. For even larger fluctuations, $\Delta_\zeta^2 \gtrsim 10^{-2}$, primordial black holes (PBH) can form, leading to interesting observational signatures [5, 6]. Given this, it is interesting to look for mechanisms that can naturally lead to a ‘blue-tilted’, enhanced power spectrum at small scales.

In models involving a single dynamical field during inflation, such an enhancement can come, for example, from an inflection point on the inflaton potential or an ultra-slow roll phase [7–11].¹ However, for any generic structure of the inflaton potential, a power spectrum that is blue-tilted at small scales can naturally arise if there are additional light scalar fields other than the inflaton field. One class of such mechanisms involves a rolling complex scalar field where the radial mode φ has a mass of order the inflationary Hubble scale H and is initially displaced away from the minimum [13]. As φ rolls down the inflationary potential, the fluctuations of the Goldstone mode $\propto (H/\varphi)^2$ increase with time. This can then give rise to *isocurvature* fluctuations that increase with k , i.e., a blue-tilted spectrum. This idea was further discussed in [14] to show how *curvature* perturbations can be enhanced on small scales as well, and lead to the formation of PBH. For further studies on blue-tilted isocurvature perturbations, see, e.g., [15–18]. Other than this, models of vector DM [19], early matter domination [20], and incomplete phase transitions [21] can also give rise to enhanced curvature perturbation at small scales.

In this work, we focus on a different mechanism where a Hubble-mass scalar field quantum mechanically fluctuates around the minimum of its potential, instead of being significantly displaced away from it (as in [13, 14]).² Hubble-mass fields can naturally roll down to their minimum since the homogeneous field value decreases with time as $\exp(-m^2 t/(3H))$, where m is the mass of the field with $m \lesssim H$. Given that we do not know the *total* number of e -foldings that took place during inflation, it is plausible that a Hubble mass particle was already classically driven to the minimum of the potential when the CMB-observable modes exit the horizon during inflation. For example, for $m^2/H^2 = 0.2$, the field value decreases by approximately a factor of 10^3 , for 100 e -foldings of inflation prior to the exit of the CMB-observable modes. For any initial field value $\varphi_{\text{ini}} \lesssim 10^3 \langle \varphi \rangle$, this can then naturally localize the massive field near the minimum

$\langle \varphi \rangle$. However, the field can still have quantum mechanical fluctuations which tend to diffuse the field away from $\langle \varphi \rangle$. The potential for the field, on the other hand, tries to push the field back to $\langle \varphi \rangle$. The combination of these two effects gives rise to a non-trivial probability distribution for the field, both as a function of time and space.

We study these effects using the stochastic formalism [23, 24] for light scalar fields in de Sitter (dS) space-time. In particular, such stochastic effects can lead to a spectrum that is blue-tilted at small scales. While we carry out the computation by solving the associated Fokker-Planck equation in detail below, we can intuitively understand the origin of a blue-tilted spectrum as follows. For simplicity, we momentarily restrict our discussion to a free scalar field σ with mass m such that $m^2 \lesssim H^2$. The fluctuation $\sigma_k(t)$, corresponding to a comoving k -mode, decays after horizon exit as $\sigma_k(t) \sim H \exp(-m^2(t - t_*)/(3H))$, where t_* is the time when the mode exits the horizon, $k = a(t_*)H$. We can rewrite the above by noting that physical momenta redshift as a function of time via $k/a(t) = H \exp(-H(t - t_*))$. Then we arrive at, $\sigma_k(t) \sim H(k/(aH))^{m^2/(3H^2)}$. Therefore, the dimensionless power spectrum, $|\sigma_k|^2 k^3 \propto (k/(aH))^{2m^2/(3H^2)}$ has a blue tilt of $2m^2/(3H^2)$. Physically, modes with smaller values of k exit the horizon earlier and get more diluted compared to modes with larger values of k , leading to more power at larger k , and thus a blue-tilted spectrum. This qualitative feature, including the specific value of the tilt for a free field, is reproduced by the calculation described later where we also include the effects of a quartic self-coupling. We summarize the mechanism in Fig. 1.

We note that if m is significantly smaller than H , the tilt is reduced and the observational signatures are less striking. On the other hand, for $m \gtrsim H$, the field is exponentially damped, and stochastic effects are not efficient in displacing the field away from the minimum. Therefore, it is puzzling as to why the particle mass, a priori arbitrary, could be close to H in realistic scenarios. However, a situation with $m \approx H$ can naturally arise if the field is non-minimally coupled to gravity. That is, a coupling $\mathcal{L} \supset cR\sigma^2$, where R is the Ricci scalar, can uplift the particle mass during inflation $m^2 = (c/12)H^2$, regardless of a smaller ‘bare’ mass. Here we have used $R = (1/12)H^2$ during inflation, and we notice for $c \sim \mathcal{O}(1)$, we can have a non-negligible blue-tilted spectrum.

The way the spectrum of σ affects the curvature perturbation depends on the cosmology, and in particular, the lifetime of σ . During inflation, the energy density stored in σ is of order H^4 , as expected, since σ receives H -scale quantum fluctuations. This is subdominant compared to the energy stored in the inflaton field $\sim H^2 M_{\text{pl}}^2$. This implies σ acts as a spectator field during inflation, and through the stochastic effects, σ obtains isocurvature fluctuations. After the end of inflation, σ dilutes as matter while the inflaton decay products dilute as radiation. Therefore, similar to the curvaton paradigm [25–28], the fractional energy density in σ increases with time. Even-

¹ See also [12] for PBH formation in a multi-field ultra-slow roll inflationary model.

² For scenarios where the spectator field fluctuates around the minimum and gives rise to dark matter abundance, see, e.g., [22].

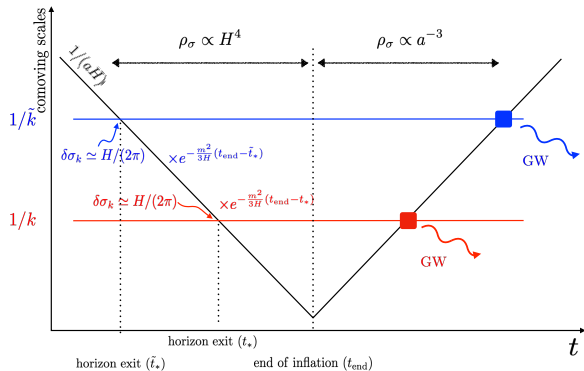


Figure 1. Schematic of the mechanism. The comoving horizon $1/(aH)$ decreases during inflation and increases after that. Any k -mode carries a fluctuation of order $H/(2\pi)$ at the time of mode exit. However, modes with larger k (red) exit the horizon later and encounters less dilution compared to modes with smaller k (blue), since $t_* > \tilde{t}_*$. Consequently, modes with larger k source stronger gravitational waves upon horizon re-entry (shown via square box). We also depict the fact that σ carries an energy density $\propto H^4$ during inflation, and dilutes as matter (for our benchmark choices) after inflation ends.

tually, σ decays into Standard Model radiation, and its isocurvature perturbations get imprinted onto the curvature perturbation. Different from the curvaton paradigm, in our scenario, σ does not dominate the energy density of the Universe, and also the fluctuations of the inflaton are not negligible. In particular, on large scales, observed via CMB and LSS, the fluctuations are red-tilted and sourced by the inflaton, as in Λ CDM cosmology. On the other hand, the blue-tilted σ fluctuations are subdominant on those scales, while dominant at smaller scales \lesssim Mpc. These enhanced perturbations can source an SGWB, observable in future gravitational wave detectors, as we describe below.

The rest of the work is organized as follows. In section II, we describe the evolution of the inflaton field and σ along with some general properties of curvature perturbation in our framework. In section III, we compute the stochastic contributions to σ fluctuations to obtain its power spectrum. We then use these results in section IV to determine the full shape of the curvature power spectrum, both on large and small scales. The small-scale enhancement of the curvature power spectrum leads to an observable SGWB and we evaluate the detection prospects in section V in the context of μ -Hz to Hz-scale gravitational wave detectors. We conclude in section VI. We include some technical details relevant to the computation of SGWB in appendix A.

II. COSMOLOGICAL HISTORY AND CURVATURE PERTURBATION

We now describe in detail the cosmological evolution considered in this work. We assume that the inflaton field ϕ drives the expansion of the Universe during inflation and the quantum fluctuations of ϕ generate the density fluctuations that we observe in the CMB and LSS, as in standard cosmology. We also assume that there is a second real scalar field σ which behaves as a subdominant spectator field during inflation, as alluded to above. We parametrize its potential as,

$$V(\sigma) = \frac{1}{2}m^2\sigma^2 + \frac{1}{4}\lambda\sigma^4. \quad (1)$$

The σ field does not drive inflation but nonetheless obtains quantum fluctuations during inflation. In particular, σ obtains stochastic fluctuations around the minimum of its potential, as we compute in section III. After the end of inflation, the inflaton is assumed to reheat into radiation with energy density ρ_r , which dominates the expansion of the Universe.

On the other hand, the evolution of the σ field depends on its mass m , interaction λ , and its frozen (root mean squared) displacement σ_0 during inflation. As long as the ‘effective’ mass of σ : $m^2 + 3\lambda\sigma_0^2$, is smaller than the Hubble scale, σ remains approximately frozen at σ_0 . However, after the Hubble scale falls below the effective mass, σ starts oscillating around its potential. The evolution of its energy density ρ_σ , during this oscillatory phase depends on the values of m and λ . If the quartic interactions dominate, with $\lambda\sigma^2 \gg m^2$, ρ_σ dilutes like radiation [29]. Eventually, the amplitude of σ decreases sufficiently, so that $\lambda\sigma^2 \lesssim m^2$, following which ρ_σ starts redshifting like matter. We illustrate these behaviors in Fig. 2.

Similar to the curvaton paradigm [25–28], during the epoch ρ_σ is diluting as matter, its fractional energy density, $f_\sigma(t) \equiv \rho_\sigma(t)/\rho_r(t)$, increases linearly with the scale factor $a(t)$. For our benchmark parameter choices, we assume σ to decay into SM radiation while $f_\sigma(t_d) \sim 1$, where t_d denotes the time of σ decay. After t_d , the evolution of the Universe coincides with standard cosmology.

With this cosmology in mind, we can track the evolution of various cosmological perturbations using the gauge invariant quantity ζ , the curvature perturbation on uniform-density hypersurfaces [30],

$$\zeta = -\psi - H \frac{\delta\rho}{\dot{\rho}}. \quad (2)$$

Here ψ is a fluctuation appearing in the spatial part of the metric as, $\delta g_{ij} = -2a^2\psi\delta_{ij}$ (ignoring vector and tensor perturbations), $\delta\rho$ denotes a fluctuation around a homogeneous density ρ , and an overdot denotes a derivative with respect to physical time t . We assume that the decay products of ϕ do not interact with σ during their cosmological evolution. Since there is no energy transfer

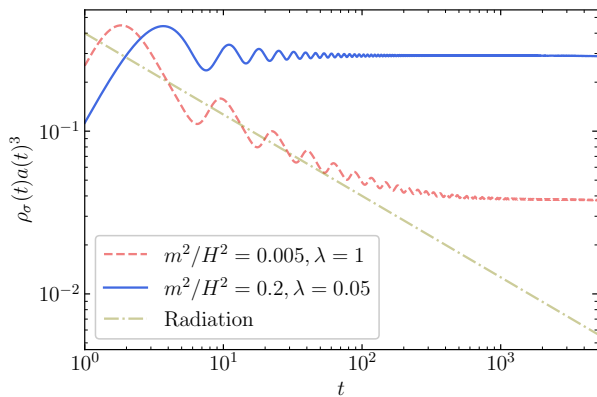


Figure 2. Time evolution of scalar field energy density $\rho_\sigma(t)$. In scenarios where the quartic term dominates the initial evolution (dashed red), the field dilutes as radiation (dot-dashed olive), $\rho_\sigma(t) \propto 1/a(t)^4$. Eventually, the mass term becomes important, and the behavior becomes $\rho_\sigma(t) \propto 1/a(t)^3$. The benchmark choices in this work will mimic the blue curve where the evolution of $\rho_\sigma(t)$ is always dominated by the mass term with a matter-like dilution. For both the blue and the red curves, $t = 1$ corresponds to the moment when the Hubble scale is approximately equal to the effective mass and the field starts oscillating.

between the two sectors, their energy densities evolve as,

$$\dot{\rho}_r = -4H\rho_r, \quad \dot{\rho}_\sigma = -3H\rho_\sigma, \quad (3)$$

where we have focused on the epoch where σ dilutes like matter. For the benchmark parameter choices discussed below, the matter-like dilution for σ onsets soon after inflation. Similar to eq. (2), we can parametrize gauge invariant fluctuations in radiation and σ with the variables,

$$\zeta_r = -\psi + \frac{1}{4} \frac{\delta\rho_r}{\rho_r}, \quad \zeta_\sigma = -\psi + \frac{1}{3} \frac{\delta\rho_\sigma}{\rho_\sigma}. \quad (4)$$

In terms of the above variables, we can express eq. (2) as,

$$\zeta = \frac{4}{4+3f_\sigma} \zeta_r + \frac{3f_\sigma}{4+3f_\sigma} \zeta_\sigma = \zeta_r + \frac{f_\sigma}{4+3f_\sigma} S_\sigma. \quad (5)$$

Here $S_\sigma \equiv 3(\zeta_\sigma - \zeta_r)$ is the isocurvature perturbation between radiation and σ perturbations. In the absence of any energy transfer, ζ_r and ζ_σ are each conserved at super-horizon scales [31]. As a result, the evolution of ζ is entirely determined by the time-dependent relative energy density of between radiation and σ , $f_\sigma = \rho_\sigma/\rho_r$. Since ζ_r and S_σ are uncorrelated, the power spectrum for curvature perturbation $\langle \zeta(\mathbf{k})\zeta(\mathbf{k}') \rangle \equiv (2\pi)^3 \delta(\mathbf{k} + \mathbf{k}') P_\zeta(k)$ is determined by,

$$P_\zeta(k) = P_{\zeta_r}(k) + \left(\frac{f_\sigma}{4+3f_\sigma} \right)^2 P_{S_\sigma}(k), \quad (6)$$

or equivalently,

$$\Delta_\zeta^2(k) = \Delta_{\zeta_r}^2(k) + \left(\frac{f_\sigma}{4+3f_\sigma} \right)^2 \Delta_{S_\sigma}^2(k), \quad (7)$$

where $\Delta_\zeta^2(k) = k^3 P_\zeta(k)/(2\pi^2)$, with $\Delta_{\zeta_r}^2(k)$ and $\Delta_{S_\sigma}^2(k)$ defined analogously.

To compute the spectral tilt, we denote the comoving momentum of the mode that enters the horizon at t_d , the time of σ decay, as k_d which satisfies $k_d = a(t_d)H(t_d)$. For $t > t_d$, ζ remains conserved with time on superhorizon scales. Correspondingly, for $k < k_d$, the spectral tilt is given by,

$$n_s - 1 \equiv \frac{d \ln \Delta_\zeta^2(k)}{d \ln k} = \frac{\Delta_{\zeta_r}^2(k)}{\Delta_\zeta^2(k)} \frac{d \ln \Delta_{\zeta_r}^2(k)}{d \ln k} + \left(\frac{f_\sigma}{4+3f_\sigma} \right)^2 \frac{\Delta_{S_\sigma}^2(k)}{\Delta_\zeta^2(k)} \frac{d \ln \Delta_{S_\sigma}^2(k)}{d \ln k}. \quad (8)$$

We will consider scenarios where the radiation energy density ρ_r originates from the inflaton, and therefore, $d \ln \Delta_{\zeta_r}^2(k)/d \ln k \approx -0.04$ determines the spectral tilt observed on CMB scales [2]. On the other hand, σ acquires stochastic fluctuations to give rise to a blue-tilted power spectrum with $d \ln \Delta_{S_\sigma}^2(k)/d \ln k \sim 0.3$, as discussed next in section III. Since we will be interested in scenarios with $f_\sigma \lesssim 1$, i.e., $(f_\sigma/(4+3f_\sigma))^2 \lesssim 0.02$, we require $\Delta_{S_\sigma}^2(k)/\Delta_\zeta^2(k) \lesssim 1$ on CMB-scales to be compatible with CMB measurements of n_s . We can also compute the running of the tilt,

$$\frac{dn_s}{d \ln k} \approx \left(\frac{f_\sigma}{4+3f_\sigma} \right)^2 \frac{\Delta_{S_\sigma}^2(k)}{\Delta_\zeta^2(k)} \left(\frac{d \ln \Delta_{S_\sigma}^2(k)}{d \ln k} \right)^2. \quad (9)$$

Our benchmark parameter choices, discussed above, thus also satisfy the CMB constraints on $dn_s/d \ln k$ [2].

III. REVIEW OF THE STOCHASTIC FORMALISM

A perturbative treatment of self-interacting light scalar fields in de Sitter (dS) spacetime is subtle due to infrared divergences. A stochastic approach [23, 24] can be used to capture the nontrivial behavior of such fields in dS. In this formalism, the super-horizon components of the fields are considered classical stochastic fields that satisfy a Langevin equation, which includes a random noise originating from the sub-horizon physics. This gives rise to a Fokker-Planck equation for the probability distribution function (PDF) of the stochastic field, which can be used to calculate correlation functions of physical observables. We now review these ideas briefly while referring the reader to refs. [23, 24, 32–35] for more details.

A. Langevin and Fokker-Planck Equations

The stochastic approach provides an effective description for the long-wavelength, superhorizon sector of the field theory by decomposing the fields into long-wavelength classical components and short-wavelength quantum operators. For instance, a light scalar field can be decomposed as

$$\begin{aligned} \sigma_{\text{tot.}}(\mathbf{x}, t) &= \sigma(\mathbf{x}, t) \\ &+ \int \frac{d^3k}{(2\pi)^3} \theta(k - \epsilon a(t)H) e^{-i\mathbf{k}\cdot\mathbf{x}} (a_{\mathbf{k}} u_k + a_{-\mathbf{k}}^\dagger u_k^*), \end{aligned} \quad (10)$$

where $\theta(\dots)$ is the Heaviside step function, a is the scale factor, H is the Hubble scale, and $\epsilon \lesssim 1$ is a constant number (not to be confused with the slow-roll parameter) which defines the boundary between long ($k < \epsilon a(t)H$) and short ($k > \epsilon a(t)H$) modes. We have also denoted the classical part of the field as $\sigma(\mathbf{x}, t)$. The quantum description of the short modes is characterized by the creation and annihilation operators $a_{\mathbf{k}}, a_{\mathbf{k}}^\dagger$ along with the mode functions $u_k(t), u_k^*(t)$.

For a light field with $|V''(\sigma)| \ll H^2$, it can be shown [23, 24, 32, 33] that the classical part of the field, $\sigma(\mathbf{x}, t)$, follows a Langevin equation

$$\dot{\sigma}(\mathbf{x}, t) = -\frac{1}{3H} V'(\sigma) + \xi(\mathbf{x}, t). \quad (11)$$

Here an overdot and a prime denote derivative with respect to time and the field, respectively. The noise ξ arises from short-scale modes,

$$\xi(\mathbf{x}, t) = \epsilon a H^2 \int \frac{d^3k}{(2\pi)^3} \delta(k - \epsilon a H) e^{-i\mathbf{k}\cdot\mathbf{x}} (a_{\mathbf{k}} u_k + a_{-\mathbf{k}}^\dagger u_k^*), \quad (12)$$

with a correlation

$$\langle \xi(\mathbf{x}_1, t_1) \xi(\mathbf{x}_2, t_2) \rangle = \frac{H^3}{4\pi^2} \delta(t_1 - t_2) j_0(\epsilon a H |\mathbf{x}_1 - \mathbf{x}_2|), \quad (13)$$

where $j_0(x) = \sin x/x$ is the zeroth order spherical Bessel function. We see that the noise is uncorrelated in time (i.e., it is a white noise), but also it is uncorrelated over spatial separations larger than $(\epsilon a H)^{-1}$.

The Langevin equation (11) gives rise to a Fokker-Planck equation for the one-point PDF,

$$\begin{aligned} \frac{\partial P_{\text{FP}}(t, \sigma(\mathbf{x}, t))}{\partial t} &= \left[\frac{V''(\sigma(\mathbf{x}, t))}{3H} \right. \\ &+ \left. \frac{V'(\sigma(\mathbf{x}, t))}{3H} \frac{\partial}{\partial \sigma} + \frac{H^3}{8\pi^2} \frac{\partial^2}{\partial \sigma^2} \right] P_{\text{FP}}(t, \sigma(\mathbf{x}, t)). \end{aligned} \quad (14)$$

Here $P_{\text{FP}}(t, \sigma(\mathbf{x}, t))$ is the PDF of the classical component to take the value $\sigma(\mathbf{x}, t)$ at time t . Thus the Fokker-Planck equation describes how an ensemble of field configurations evolves as a function of time, according to the underlying Langevin equation. In this equation, the first and second terms on the right-hand side represent classical drift terms that depend on the potential $V(\sigma)$. The

third term represents a diffusion contribution from the noise ξ . While the classical drift tries to move the central value of the field towards the minimum of the potential, the diffusion contribution pushes the field away from the minimum. An equilibrium is achieved when these two effects balance each other. This equilibrium solution can be obtained by setting $\partial P_{\text{FP}}/\partial t = 0$ in (14), and is given by

$$P_{\text{FP,eq}}(\sigma) = \frac{1}{\mathcal{N}} \exp\left(-\frac{8\pi^2}{3H^4} V(\sigma)\right), \quad (15)$$

where \mathcal{N} is a normalization constant. Upon a variable change

$$\tilde{P}_{\text{FP}}(t, \sigma) \equiv \exp\left(\frac{4\pi^2 V(\sigma)}{3H^4}\right) P_{\text{FP}}(t, \sigma), \quad (16)$$

eq. (14) can be written as

$$\frac{\partial \tilde{P}_{\text{FP}}(t, \sigma)}{\partial t} = \frac{H^3}{4\pi^2} \underbrace{\left[-\frac{1}{2} (v'^2 - v'') + \frac{1}{2} \frac{\partial^2}{\partial \sigma^2} \right]}_{D_\sigma} \tilde{P}_{\text{FP}}(t, \sigma), \quad (17)$$

with $v(\sigma) = 4\pi^2 V(\sigma)/(3H^4)$. We can recast the above as an eigenvalue equation. To that end, we write

$$\tilde{P}_{\text{FP}}(t, \sigma) = \sum_n a_n e^{-\Lambda_n t} \psi_n(\sigma), \quad (18)$$

where $\psi_n(\sigma)$ satisfies the equation

$$D_\sigma \psi_n(\sigma) = -\frac{4\pi^2}{H^3} \Lambda_n \psi_n(\sigma). \quad (19)$$

The eigenfunctions $\psi_n(\sigma)$ form an orthonormal basis of functions and a_n 's are some arbitrary coefficients.

This time-independent eigenvalue equation (19) can be solved numerically for a generic potential $V(\sigma)$, as we discuss below with an example. By definition, and independent of the form of the potential, the eigenfunction ψ_0 corresponding to the eigenvalue $\Lambda_0 = 0$, determines the equilibrium distribution. Solution of the eq. (19) for $\Lambda_0 = 0$ is given by

$$\psi_0(\sigma) = \frac{1}{\sqrt{\mathcal{N}}} \exp\left(-\frac{4\pi^2}{3H^4} V(\sigma)\right). \quad (20)$$

Thus comparing to eq. (15) we get,

$$P_{\text{FP,eq}}(\sigma) = \psi_0(\sigma)^2. \quad (21)$$

B. Two-point Correlation Function and Power Spectrum

We are interested in calculating the two-point correlation functions of cosmological perturbations. Any such two-point correlation function depends only on the

geodesic distance s between the two points. Given the coordinates of the two points (\mathbf{x}_1, t_1) and (\mathbf{x}_2, t_2) , this distance can be parametrized by $z = 1 + H^2 s^2/2$ with

$$z = \cosh H(t_1 - t_2) - \frac{1}{2} e^{H(t_1+t_2)} (H|\mathbf{x}_1 - \mathbf{x}_2|)^2. \quad (22)$$

To understand the significance of the variable z , we first write the two-point correlation function for an arbitrary function of σ , $g(\sigma)$, as

$$G_g(\mathbf{x}_1, t_1; \mathbf{x}_2, t_2) = \langle g(\sigma(\mathbf{x}_1, t_1))g(\sigma(\mathbf{x}_2, t_2)) \rangle. \quad (23)$$

To compute this, it is more convenient to calculate the temporal correlation first, and then use the fact that equal-time correlations over spatially separated points are related to the temporal correlation through the de Sitter-invariant variable z (22). In particular, for coincident points G_g is a function of $(t_1 - t_2)$ only, which can be expressed in terms of z for large $|z|$ as,

$$G_g(t_1 - t_2) \approx G_g(H^{-1} \ln |2z|). \quad (24)$$

However, for an equal time correlation function we can also write,

$$|2z| \approx (He^{Ht} |\mathbf{x}_1 - \mathbf{x}_2|)^2, \quad (25)$$

which gives,

$$G_g(t_1 - t_2) \simeq G_g\left(\frac{\ln |2z|}{H}\right) \simeq G_g\left(\frac{2}{H} \ln(aH|\mathbf{x}_1 - \mathbf{x}_2|)\right), \quad (26)$$

where the approximations hold as long as $|z| \gg 1$ and we used $a(t) = \exp(Ht)$.

Now we aim at formally calculating $G_g(t)$ in terms of solutions of the Fokker-Planck equation. The temporal correlation can be written as (see, e.g., [23, 24, 35])

$$G_g(t) = \int d\sigma \int d\sigma_0 P_{\text{FP,eq}}(\sigma_0) g(\sigma_0) \Pi(t, \sigma; \sigma_0) g(\sigma), \quad (27)$$

where $\Pi(t, \sigma; \sigma_0)$ is the kernel function of the time evolution of the probability distribution function, i.e., if the probability distribution is $\delta(\sigma - \sigma_0)$ at $t = 0$ it would be $\Pi(t, \sigma; \sigma_0)$ at time t . In particular, it is defined by

$$P_{\text{FP}}(t; \sigma) = \int d\sigma_0 \Pi(t, \sigma; \sigma_0) P(0; \sigma_0). \quad (28)$$

In terms of re-scaled probabilities, we can rewrite the above as,

$$\tilde{P}_{\text{FP}}(t; \sigma) = \int d\sigma_0 \tilde{\Pi}(t, \sigma; \sigma_0) \tilde{P}_{\text{FP}}(0; \sigma_0), \quad (29)$$

$$\Pi(t, \sigma; \sigma_0) = e^{-v(\sigma)} \tilde{\Pi}(t, \sigma; \sigma_0) e^{v(\sigma_0)}. \quad (30)$$

It follows that $\tilde{\Pi}$ satisfies the same Fokker-Planck equation as \tilde{P}_{FP} (17). Therefore, the solutions can be written as

$$\tilde{\Pi}(t; \sigma, \sigma_0) = \sum_n \psi_n(\sigma_0) e^{-\Lambda_n t} \psi_n(\sigma), \quad (31)$$

which obeys the initial condition $\tilde{\Pi}(0; \sigma, \sigma_0) = \delta(\sigma - \sigma_0)$ is satisfied. Therefore, according to (27) we have³

$$G_g(t) = \sum_n \int d\sigma_0 \psi_0(\sigma_0) g(\sigma_0) \psi_n(\sigma_0) e^{-\Lambda_n t} \\ \times \int d\sigma \psi_n(\sigma) g(\sigma) \psi_0(\sigma) = \sum_n g_n^2 e^{-\Lambda_n t}, \quad (32)$$

where

$$g_n \equiv \int d\sigma \psi_n(\sigma) g(\sigma) \psi_0(\sigma). \quad (33)$$

We see that in late times the correlation is dominated by the smallest $\Lambda_n \neq 0$.

We can now present the equal-time correlation function by combining (26) and (32) [23, 24, 35]:

$$G_g(|\mathbf{x}_1 - \mathbf{x}_2|) = \sum_n \frac{g_n^2}{(aH|\mathbf{x}_1 - \mathbf{x}_2|)^{2\Lambda_n/H}}. \quad (34)$$

We note that this depends on the physical distance between the two points at time t , namely, $a|\mathbf{x}_1 - \mathbf{x}_2|$. This correlation function has the following dimensionless power spectrum [35],

$$\Delta_g^2(k) = \frac{k^3}{2\pi^2} P_g(k) = \frac{k^3}{2\pi^2} \int d^3r e^{-i\mathbf{k}\cdot\mathbf{r}} G_g(r) \\ = \sum_n \frac{2g_n^2}{\pi} \Gamma\left(2 - \frac{2\Lambda_n}{H}\right) \sin\left(\frac{\pi\Lambda_n}{H}\right) \left(\frac{k}{aH}\right)^{2\Lambda_n/H} \quad (35)$$

where Γ denotes the gamma function. This expression is valid in the limit $k \ll aH$. So far our discussion has been general and is valid for any potential under the slow-roll approximation and the assumption of a small effective mass, $|V''(\sigma)| \ll H^2$. In the next section, we discuss a concrete example with $V(\sigma)$ given in eq. (1).

IV. LARGE CURVATURE PERTURBATION FROM STOCHASTIC FLUCTUATIONS

We focus on the potential in eq. (1) to demonstrate how large curvature perturbation can arise from stochastic fluctuations. We first describe various equilibrium quantities and how to obtain the power spectra $P_{\mathcal{S}_\sigma}$, and consequently evaluate P_ζ which determines the strength of the GW signal.

A. Equilibrium Configuration

The normalized PDF for the one-point function is given by eq. (15). For convenience, we reproduce it here

$$P_{\text{FP,eq}}(\sigma) = \frac{1}{\mathcal{N}} \exp\left(-\frac{8\pi^2 V(\sigma)}{3H^4}\right), \quad (36)$$

³ Note that $P_{\text{FP,eq}}(\sigma_0) = \psi_0(\sigma_0)^2 = \psi_0(\sigma_0)\psi_0(\sigma) e^{4\pi^2 V(\sigma)/3H^4} e^{-4\pi^2 V(\sigma_0)/3H^4}$.

with

$$\mathcal{N} = \frac{2\sqrt{2}\sqrt{\lambda}}{\exp\left(\frac{m^4\pi^2}{3H^4\lambda}\right) m K_{\frac{3}{4}}\left(\frac{m^4\pi^2}{3H^4\lambda}\right)}. \quad (37)$$

Here $K_n(x)$ is the modified Bessel function of the second kind. The mean displacement of the field can be computed as,

$$\langle\sigma^2\rangle = \int_0^\infty d\sigma \sigma^2 P_{\text{FP,eq}}(\sigma) = \frac{m^2}{2\lambda} \left(-1 + \frac{K_{\frac{3}{4}}\left(\frac{m^4\pi^2}{3H^4\lambda}\right)}{K_{\frac{1}{4}}\left(\frac{m^4\pi^2}{3H^4\lambda}\right)} \right). \quad (38)$$

In the appropriate limits, this can be simplified to,

$$\langle\sigma^2\rangle \Big|_{\lambda \rightarrow 0} = \frac{3H^4}{8\pi^2 m^2}, \quad (39)$$

$$\langle\sigma^2\rangle \Big|_{m \rightarrow 0} = \sqrt{\frac{3}{2\lambda}} \frac{\Gamma(3/4)}{\Gamma(1/4)\pi} H^2, \quad (40)$$

matching the standard results [24]. We can also compute the average energy density of the field as,

$$\begin{aligned} \langle V(\sigma) \rangle &= \int_0^\infty d\sigma V(\sigma) P_{\text{FP,eq}}(\sigma) \\ &= \frac{1}{32} \left(\frac{3H^4}{\pi^2} - \frac{4m^4}{\lambda} + \frac{4m^4}{\lambda} \frac{K_{\frac{3}{4}}\left(\frac{m^4\pi^2}{3H^4\lambda}\right)}{K_{\frac{1}{4}}\left(\frac{m^4\pi^2}{3H^4\lambda}\right)} \right), \end{aligned} \quad (41)$$

reducing to,

$$\langle V(\sigma) \rangle \Big|_{\lambda \rightarrow 0} = \frac{3H^4}{16\pi^2}, \quad (42)$$

$$\langle V(\sigma) \rangle \Big|_{m \rightarrow 0} = \frac{3H^4}{32\pi^2}. \quad (43)$$

To ensure that σ does not dominate energy density during inflation, we require

$$\langle V(\sigma) \rangle \ll 3H^2 M_{\text{pl}}^2. \quad (44)$$

Finally, we compute $\langle V''(\sigma) \rangle$ to check the validity of slow-roll of the σ field,

$$\begin{aligned} \langle V''(\sigma) \rangle &= \int_0^\infty d\sigma V''(\sigma) P_{\text{FP,eq}}(\sigma) \\ &= \frac{1}{2} m^2 \left(-1 + \frac{3K_{\frac{3}{4}}\left(\frac{m^4\pi^2}{3H^4\lambda}\right)}{K_{\frac{1}{4}}\left(\frac{m^4\pi^2}{3H^4\lambda}\right)} \right), \end{aligned} \quad (45)$$

which reduces to,

$$\langle V''(\sigma) \rangle \Big|_{\lambda \rightarrow 0} = m^2, \quad (46)$$

$$\langle V''(\sigma) \rangle \Big|_{m \rightarrow 0} = \frac{3\sqrt{3}\Gamma(3/4)}{\sqrt{2\pi}\Gamma(1/4)} \sqrt{\lambda} H^2 \approx 0.4\sqrt{\lambda} H^2. \quad (47)$$

To ensure slow-roll, we require

$$\langle V''(\sigma) \rangle \ll H^2. \quad (48)$$

m^2/H^2	λ	Λ_2/H	g_2^2	Λ_4/H	g_4^2
0.2	0.05	0.16	1.99	0.37	0.03
0.2	0.07	0.17	1.98	0.40	0.05
0.2	0.1	0.18	1.98	0.44	0.07
0.25	0.05	0.19	1.99	0.42	0.02
0.25	0.07	0.20	1.99	0.45	0.03
0.25	0.1	0.21	1.98	0.49	0.05
0.3	0.05	0.22	1.99	0.48	0.01
0.3	0.07	0.23	1.99	0.51	0.02
0.3	0.1	0.24	1.99	0.54	0.03

Table I. Eigenvalues for some benchmark parameter choices corresponding to the potential in eq. (1).

B. Power Spectrum

To obtain isocurvature power spectrum, P_{S_σ} , we need to compute the two-point function of $\delta\rho_\sigma/\rho_\sigma$. We can write this more explicitly as,

$$\frac{\delta\rho_\sigma(\mathbf{x})}{\rho_\sigma} = \frac{\rho_\sigma(\mathbf{x}) - \langle\rho_\sigma(\mathbf{x})\rangle}{\langle\rho_\sigma(\mathbf{x})\rangle} = \frac{\rho_\sigma(\mathbf{x})}{\langle\rho_\sigma(\mathbf{x})\rangle} - 1. \quad (49)$$

where we can approximate $\rho_\sigma \approx V(\sigma)$, since $\langle V(\sigma) \rangle$ is approximately frozen, as long as eq. (48) is satisfied. Referring to eq. (33) and eq. (35), the relevant coefficient g_n for ρ_σ is determined by,

$$g_n = \frac{\int d\sigma \psi_n(\sigma) \rho_\sigma \psi_0(\sigma)}{\int d\sigma \psi_0(\sigma) \rho_\sigma \psi_0(\sigma)}. \quad (50)$$

For $n > 0$, the last term in eq. (49) does not contribute because of the orthogonality of the eigenfunctions.

The eigenfunctions ψ_n and the eigenvalues Λ_n relevant for eq. (35) can be obtained by solving the eigensystem for the potential eq. (1). In terms of variables, $z = \lambda^{1/4}\sigma/H$ and $\alpha = m^2/(\sqrt{\lambda}H^2)$, the eigenvalue eq. (19) can be written as [35],

$$\begin{aligned} \frac{\partial^2 \psi_n}{\partial z^2} + \left(-\left(\frac{4\pi^2}{3}\right)^2 (\alpha z + z^3)^2 + \frac{4\pi^2}{3} (\alpha + 3z^2) \right) \psi_n \\ = -\frac{8\pi^2}{\sqrt{\lambda}} \frac{\Lambda_n}{H} \psi_n. \end{aligned} \quad (51)$$

Given the potential in eq. (1), the eigenfunctions are odd (even) functions of σ for odd (even) values of n . Since ρ_σ is an even function of σ , eq. (50) implies $g_1 = 0$, and therefore, the leading coefficient is g_2 with the eigenvalue Λ_2 determining the first non-zero contribution to the spectral tilt. We show the numerical results for the eigenvalues for some benchmark parameter choices in Table I.

The curvature power spectrum Δ_ζ^2 depends on both $\Delta_{S_\sigma}^2$ and f_σ , as in eq. (7). With the values of g_n, Λ_n in

Table I, we can compute the dimensionless power spectrum $\Delta_{S_\sigma}^2$ using eq. (35), where we can evaluate the factor of $a\dot{H}$ at the end of inflation. Furthermore, for our benchmark parameter choices, only the eigenvalue Λ_2 is relevant. Therefore, eq. (35) can be simplified as,

$$\Delta_{S_\sigma}^2(k) \approx \frac{2g_2^2}{\pi} \Gamma\left(2 - \frac{2\Lambda_2}{H}\right) \sin\left(\frac{\pi\Lambda_2}{H}\right) \left(\frac{k}{k_{\text{end}}}\right)^{2\Lambda_2/H}, \quad (52)$$

where $k_{\text{end}} = a_{\text{end}}H_{\text{end}}$.

The precise value of k_{end} depends on the cosmological history after the CMB-observable modes exit the horizon. It is usually parametrized as the number of e -foldings $N(k) \equiv \ln(a_{\text{end}}/a_k)$, where a_k is the scale factor when a k -mode exits the horizon during inflation, defined by $k = a_k H_k$. Assuming an equation of state parameter w between the end of inflation and the end of the reheating phase, we can derive the relation [36, 37],

$$\frac{k}{a_0 H_0} = \left(\frac{\sqrt{\pi} T_0}{90^{1/4} H_0}\right) e^{-N(k)} \left(\frac{V_k^{1/2}}{\rho_{\text{end}}^{1/4} M_{\text{pl}}}\right) \left(\frac{\rho_{\text{RH}}}{\rho_{\text{end}}}\right)^{\frac{1-3w}{12(1+w)}} \times \frac{g_{*,s,0}^{1/4} g_{*,\text{RH}}^{1/3}}{g_{*,s,\text{RH}}^{1/3}}. \quad (53)$$

Here $g_{*,\text{RH}}$ and $g_{*,s,\text{RH}}$ are the effective number of degrees of freedom in the energy density and entropy density, respectively, at the end of the reheating phase; V_k is the inflationary energy density when the k -mode exits the horizon; ρ_{end} and ρ_{RH} are the energy densities at the end of inflation and reheating, respectively. Plugging in the CMB temperature T_0 and the present-day Hubble parameter H_0 , we arrive at

$$N(k) \approx 67 - \ln\left(\frac{k}{a_0 H_0}\right) + \ln\left(\frac{V_k^{1/2}}{\rho_{\text{end}}^{1/4} M_{\text{pl}}}\right) + \frac{1-3w}{12(1+w)} \ln\left(\frac{\rho_{\text{RH}}}{\rho_{\text{end}}}\right) + \ln\left(\frac{g_{*,\text{RH}}^{1/4}}{g_{*,s,\text{RH}}^{1/3}}\right). \quad (54)$$

Significant sources of uncertainty in $N(k)$ comes from V_k , ρ_{end} , ρ_{RH} , and w . Furthermore, eq. (54) assumes a standard cosmological history where following reheating, the Universe becomes radiation dominated until the epoch of matter-radiation equality. We now consider some benchmark choices with which we can evaluate $N(k)$. We set $k = a_0 H_0$, assume $V_k^{1/4} = 10^{16}$ GeV, close to the current upper bound [2], $\rho_{\text{end}} \simeq V_k/100$, motivated by simple slow-roll inflation models, and $w \approx 0$ [38–40].⁴ Then depending on the reheating temperature, we get

$$N(k) = \begin{cases} 62, & T_{\text{RH}} = 6 \times 10^{15} \text{ GeV}, \\ 59, & T_{\text{RH}} = 10^{11} \text{ GeV}. \end{cases} \quad (55)$$

⁴ The precise value of w is model dependent, see, e.g., [41–45] and [46] for a review.

For the first benchmark, we have assumed an instantaneous reheating after inflation, while for the second benchmark, the reheating process takes place for an extended period of time. For these two benchmarks, $k_{\text{end}} \approx 4 \times 10^{23} \text{ Mpc}^{-1}$ and 10^{22} Mpc^{-1} , respectively.

To determine $\Delta_\zeta^2(k)$, we also need to evaluate f_σ as a function of time. We can express the time dependence of f_σ in terms of k in the following way. A given k -mode re-enters the horizon when $k = a_k H_k$, and assuming radiation domination, we get $k/k_{\text{end}} = a_{\text{end}}/a_k$. Since f_σ increases with the scale factor before σ decay, we can express $f_\sigma(t) = f_\sigma(t_d)(k_d/k)$, for $t < t_d$, where k_d and t , respectively. Therefore, the final expression for the curvature power spectrum at the time of mode re-entry follows from eq. (7),

$$\Delta_\zeta^2(k) = \begin{cases} \Delta_{\zeta_r}^2(k) + \left(\frac{f_\sigma(t_d)}{4+3f_\sigma(t_d)}\right)^2 \Delta_{S_\sigma}^2(k), & k < k_d, \\ \Delta_{\zeta_r}^2(k) + \left(\frac{f_\sigma(t_d)(k_d/k)}{4+3f_\sigma(t_d)(k_d/k)}\right)^2 \Delta_{S_\sigma}^2(k), & k > k_d. \end{cases} \quad (56)$$

To determine the scale k_d , we consider the benchmarks discussed above, along with some additional choices for other parameters.

a. Benchmark 1. We focus on the first benchmark in eq. (55). For $m^2 = 0.2H^2$ and $\lambda \simeq 0.05 - 0.1$, we get $\langle V(\sigma) \rangle \approx 0.02H^4$ from eq. (41), implying $\langle V(\sigma) \rangle/V_k \approx 3 \times 10^{-12}$ for $H = 5 \times 10^{13}$ GeV. Assuming instantaneous reheating, and $\rho_{\text{end}} \simeq V_k/100$, we see $f_\sigma \simeq 1$ for $a \simeq (1/3) \times 10^{10} a_{\text{end}}$. As benchmarks, we assume σ decays when $f_\sigma = 1$ and $1/3$. Using $k_{\text{end}} \approx 4 \times 10^{23} \text{ Mpc}^{-1}$, we can then evaluate $k_d \approx 10^{14} \text{ Mpc}^{-1}$ and $k_d \approx 3 \times 10^{14} \text{ Mpc}^{-1}$, respectively. The result for the curvature power spectrum with these choices is shown in Fig. 3 (left).

b. Benchmark 2. We now discuss the second benchmark in eq. (55). We again choose $m^2 = 0.2H^2$ and $\lambda \simeq 0.05 - 0.1$, for which we get $\langle V(\sigma) \rangle \approx 0.02H^4$ from eq. (41). This implies $\langle V(\sigma) \rangle/V_k \approx 3 \times 10^{-12}$ for $H = 5 \times 10^{13}$ GeV, as before. The rest of the parameters can be derived in an analogous way, with one difference. During the reheating epoch, with our assumption $w \approx 0$, f_σ does not grow with the scale factor since the dominant energy density of the Universe is also diluting as matter. Accounting for this gives $k_d \approx 8 \times 10^{11} \text{ Mpc}^{-1}$ and $k_d \approx 3 \times 10^{12} \text{ Mpc}^{-1}$, for $f_\sigma = 1$ and $1/3$, respectively, with the resulting curvature power spectrum shown in Fig. 3 (center).

c. Benchmark 3. This is same as the first benchmark discussed above, except we focus on $m^2 = 0.25H^2$ and $0.3H^2$ along with $f_\sigma = 1$. The result is shown in Fig. 3 (right).

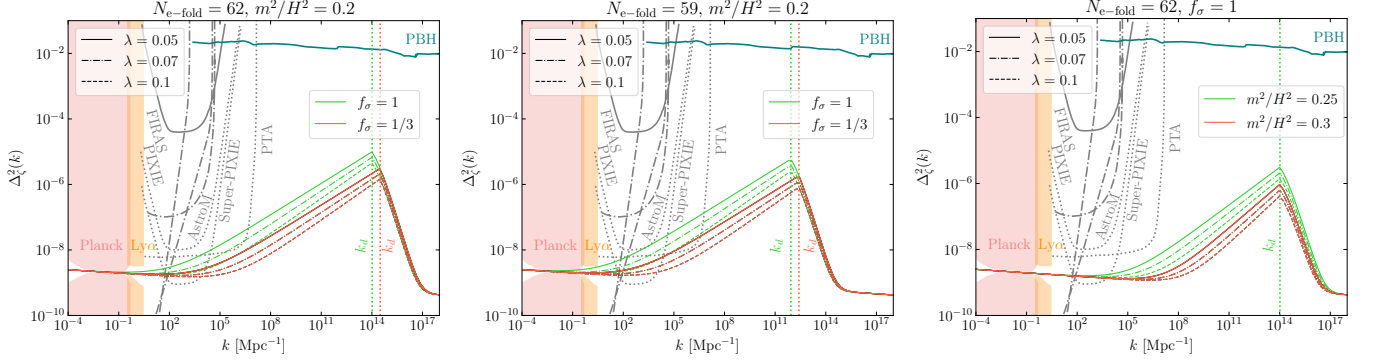


Figure 3. Power spectrum of curvature perturbations for the benchmarks discussed above. Stochastic effects lead to a blue-tilted spectrum of σ , with larger m and λ corresponding to larger tilts, leading to faster decay as k gets smaller. The blue-tilt is eventually cut off at k_d , the k -mode that reenters the horizon at the time of σ decay. For k larger than k_d , the fractional energy density in σ at the time of mode-reentry is smaller. Correspondingly, Δ_ζ^2 gets suppressed. Eventually, for very large k , the effects of σ become negligible, and Δ_ζ^2 reverts back to its standard, slightly red-tilted behavior. A smaller value of $f_\sigma(k_d)$, the fractional energy density at the time σ decay, suppresses the effect of σ to Δ_ζ^2 , and hence leads to a suppressed peak. This mechanism predicts signatures in CMB spectral distortion measurements [47], especially in Super-PIXIE [48], along with Pulsar Timing Array (PTA) probes for enhanced DM substructure [49], and precision astrometry probes (AstroM) [50]. We also show constraints from FIRAS [51] and non-observation of primordial black holes (PBH) [5].

V. GRAVITATIONAL WAVE SIGNATURE

A. Secondary Gravitational Waves from Scalar Curvature Perturbation

We now review how large primordial curvature perturbations can source GW at the second order in perturbation theory [52, 53] (for a review see [4]). We then evaluate the GW spectrum sourced by Δ_ζ^2 computed in section IV. We start our discussion with a brief review of the essential relations and expand the discussion further in appendix A.

We can write a tensor perturbation in Fourier space as,

$$h_{ij}(\tau, \mathbf{x}) = \sum_{\lambda=+, \times} \int \frac{d^3k}{(2\pi)^3} e^{i\mathbf{k}\cdot\mathbf{x}} \epsilon_{ij}^\lambda(\mathbf{k}) h_\lambda(\tau, \mathbf{k}), \quad (57)$$

where $\epsilon_{ij}^{\lambda=\{+, \times\}}(\mathbf{k})$ are polarization tensors:

$$\epsilon_{ij}^+(\mathbf{k}) = \frac{1}{\sqrt{2}} (e_{1,i}(\mathbf{k})e_{1,j}(\mathbf{k}) - e_{2,i}(\mathbf{k})e_{2,j}(\mathbf{k})), \quad (58)$$

$$\epsilon_{ij}^\times(\mathbf{k}) = \frac{1}{\sqrt{2}} (e_{1,i}(\mathbf{k})e_{2,j}(\mathbf{k}) + e_{2,i}(\mathbf{k})e_{1,j}(\mathbf{k})), \quad (59)$$

with $e_{1,2}$ the orthonormal bases spanning the plane transverse to \mathbf{k} . The equation of motion determining the generation and evolution of GW is given by

$$h_\lambda''(\tau, \mathbf{k}) + 2\mathcal{H}h_\lambda'(\tau, \mathbf{k}) + k^2h_\lambda(\tau, \mathbf{k}) = 4\mathcal{S}_\lambda(\tau, \mathbf{k}), \quad (60)$$

where $'$ denotes derivative with respect to the conformal time τ and $\mathcal{H} = a'/a$ is the conformal Hubble parameter. The second-order (in scalar metric perturbation Φ)

source term is given by⁵

$$\begin{aligned} \mathcal{S}_\lambda(\tau, \mathbf{k}) = \int \frac{d^3q}{(2\pi)^3} \frac{Q_\lambda(\mathbf{k}, \mathbf{q})}{3(1+w)} \left[2(5+3w)\Phi_{\mathbf{p}}\Phi_{\mathbf{q}} \right. \\ \left. + \tau^2(1+3w)^2\Phi'_{\mathbf{p}}\Phi'_{\mathbf{q}} + 2\tau(1+3w)(\Phi_{\mathbf{p}}\Phi'_{\mathbf{q}} + \Phi_{\mathbf{q}}\Phi'_{\mathbf{p}}) \right]. \end{aligned} \quad (62)$$

We have defined $\mathbf{p} \equiv \mathbf{k} - \mathbf{q}$, $\Phi_{\mathbf{k}} \equiv \Phi(\tau, \mathbf{k})$, and a projection operator $Q_\lambda(\mathbf{k}, \mathbf{q})$:

$$Q_\lambda(\mathbf{k}, \mathbf{q}) \equiv \epsilon_\lambda^{ij}(\mathbf{k})q_iq_j. \quad (63)$$

The metric perturbation $\Phi(\tau, \mathbf{k})$ can be written in terms of the primordial curvature perturbation $\zeta(\mathbf{k})$,

$$\Phi(\tau, \mathbf{k}) = \frac{3+3w}{5+3w} T_\Phi(k\tau)\zeta(\mathbf{k}), \quad (64)$$

via a transfer function $T_\Phi(k\tau)$ which depends on w . With the above quantities, one can now solve eq. (60) using the Green function method,⁶

$$h_\lambda(\tau, \mathbf{k}) = \frac{4}{a(\tau)} \int_{\tau_0}^{\tau} d\bar{\tau} G_{\mathbf{k}}(\tau, \bar{\tau}) a(\bar{\tau}) \mathcal{S}_\lambda(\bar{\tau}, \mathbf{k}). \quad (65)$$

⁵ We parametrize the scalar metric fluctuations, for vanishing anisotropic stress, as

$$ds^2 = -(1+2\Phi)dt^2 + a^2(1-2\Phi)\delta_{ij}dx^i dx^j \quad (61)$$

⁶ Scale factors appearing in the I integral as $a(\bar{\tau})/a(\tau)$ are the artifact of $G_{\mathbf{k}}(\tau, \bar{\tau})$ being Green's function of the new variable $v(\tau, \mathbf{k}) = ah(\tau, \mathbf{k})$ and not h_λ itself; see Appendix A 2.

Using the solutions of eq. (60), the power spectrum $P_\lambda(\tau, k)$, defined via,

$$\langle h_{\lambda_1}(\tau, \mathbf{k}_1) h_{\lambda_2}(\tau, \mathbf{k}_2) \rangle \equiv (2\pi)^3 \delta_{\lambda_1 \lambda_2} \delta^3(\mathbf{k}_1 + \mathbf{k}_2) P_{\lambda_1}(\tau, k_1), \quad (66)$$

can be written as,

$$\begin{aligned} \langle h_{\lambda_1}(\tau, \mathbf{k}_1) h_{\lambda_2}(\tau, \mathbf{k}_2) \rangle = \\ 16 \int \frac{d^3 q_1}{(2\pi)^3} \frac{d^3 q_2}{(2\pi)^3} Q_{\lambda_1}(\mathbf{k}_1, \mathbf{q}_1) Q_{\lambda_2}(\mathbf{k}_2, \mathbf{q}_2) I(|\mathbf{k}_1 - \mathbf{q}_1|, q_1, \tau_1) \\ \times I(|\mathbf{k}_2 - \mathbf{q}_2|, q_2, \tau_2) \langle \zeta(\mathbf{q}_1) \zeta(\mathbf{k}_1 - \mathbf{q}_1) \zeta(\mathbf{q}_2) \zeta(\mathbf{k}_2 - \mathbf{q}_2) \rangle. \end{aligned} \quad (67)$$

Here

$$I(p, q, \tau) = \frac{1}{a(\tau)} \int_{\tau_0}^{\tau} d\bar{\tau} G_{\mathbf{k}}(\tau, \bar{\tau}) a(\bar{\tau}) f(p, q, \bar{\tau}), \quad (68)$$

and

$$\begin{aligned} \frac{(5+3w)^2}{3(1+w)} f(p, q, \tau) = 2(5+3w) T_{\Phi}(p\tau) T_{\Phi}(q\tau) \\ + \tau^2 (1+3w)^2 T'_{\Phi}(p\tau) T'_{\Phi}(q\tau) \\ + 2\tau (1+3w) [T_{\Phi}(p\tau) T'_{\Phi}(q\tau) + T'_{\Phi}(p\tau) T_{\Phi}(q\tau)]. \end{aligned} \quad (69)$$

where $T'_{\Phi}(p\tau) = \partial T_{\Phi}(p\tau) / \partial \tau$. We note that the power spectrum is sourced by the four-point correlation function of super-horizon curvature perturbations, and is further modified by the sub-horizon evolution as encapsulated in $I(p, q, \tau)$.

The four-point function in eq. (67) has both disconnected and connected contributions, from the scalar power spectrum and trispectrum, respectively. The connected contribution usually contributes in a subdominant way compared to the disconnected piece in determining total GW energy density; see [54] for a general argument.⁷ Therefore, in the following, we focus only on the disconnected contribution, which can be written as

$$\begin{aligned} P_\lambda(\tau, k) \Big|_{\text{d}} = 32 \int \frac{d^3 q}{(2\pi)^3} Q_\lambda(\mathbf{k}, \mathbf{q})^2 I(|\mathbf{k} - \mathbf{q}|, q, \tau)^2 \\ \times P_\zeta(q) P_\zeta(|\mathbf{k} - \mathbf{q}|). \end{aligned} \quad (70)$$

For a derivation of this formula see appendix A 3.

GW signal strength can be characterized by SGWB energy density per unit logarithmic interval of frequency and normalized to the total energy density [58],

$$h^2 \Omega_{\text{GW}} = \frac{1}{\rho_{\text{tot}}} \frac{d\rho_{\text{GW}}}{d \log f} \quad (71)$$

where the present day Hubble parameter is given by $H_0 = 100h$ km/s/Mpc and $\rho_{\text{tot}} = 3M_{\text{pl}}^2 H_0^2$ is the critical energy

density in terms of the reduced Planck mass $M_{\text{pl}} \approx 2.4 \times 10^{18}$ GeV. The total energy density ρ_{GW} is given by,

$$\begin{aligned} \rho_{\text{GW}} = \frac{M_{\text{pl}}^2}{4} \int d \ln k \frac{k^3}{16\pi^2} \times \\ \sum_{\lambda} \left(\langle \dot{h}_{\lambda}(t, \mathbf{k}) \dot{h}_{\lambda}(t, -\mathbf{k}) \rangle' + \frac{k^2}{a^2} \langle h_{\lambda}(t, \mathbf{k}) h_{\lambda}(t, -\mathbf{k}) \rangle' \right), \end{aligned} \quad (72)$$

with the primes denoting the fact that momentum-conserving delta functions are factored out, $\langle h_{\lambda}(t, \mathbf{k}) h_{\lambda}(t, \mathbf{k}') \rangle = (2\pi)^3 \delta^3(\mathbf{k} + \mathbf{k}') \langle h_{\lambda}(t, \mathbf{k}) h_{\lambda}(t, -\mathbf{k}) \rangle'$. Approximating $\dot{h}_{\lambda}(t, \mathbf{k}) \approx (k/a) h_{\lambda}(t, \mathbf{k})$, we can simplify to get,⁸

$$\Omega_{\text{GW}} = \frac{1}{48} \left(\frac{k}{a(\tau)H(\tau)} \right)^2 \sum_{\lambda=+, \times} \Delta_{\lambda}^2(\tau, k), \quad (73)$$

where $\Delta_{\lambda}^2(\tau, k) = (k^3/(2\pi^2)) P_{\lambda}(\tau, k)$.

The above expression can be rewritten in form convenient for numerical evaluation (see appendix A 4 for a derivation),⁹

$$\Omega_{\text{GW}}(k) = \frac{2}{48\alpha^2} \int_0^{\infty} dt \int_{-1}^1 ds \mathcal{K}_{\text{d}}(u, v) \Delta_{\zeta}^2(uk) \Delta_{\zeta}^2(vk) \quad (74)$$

where $u = |\mathbf{k} - \mathbf{q}|/k = p/k, v = q/k, s = u - v, t = u + v - 1$, and \mathcal{K}_{d} is the kernel function following from manipulating the integrand of eq. (70). This kernel function is illustrated in fig. 4a.

We now focus on the scenario where GW is generated during a radiation dominated epoch and set $w = 1/3$. We can then write (see Appendix A 1 for details),

$$T_{\Phi}(k\tau) = \frac{9\sqrt{3}}{(k\tau)^3} \left(\sin \frac{k\tau}{\sqrt{3}} - \frac{k\tau}{\sqrt{3}} \cos \frac{k\tau}{\sqrt{3}} \right), \quad (75)$$

and plot this function in fig. 4b. We note that after entering the horizon, modes start to oscillate and decay, and as a result, the sub-horizon modes do not significantly contribute to GW generation. In fig. 4c, we confirm that at any given time $f(p, q, \tau)$ is suppressed for shorter modes that have re-entered the horizon earlier. Finally, the green function is given by (see appendix A 2 for details)

$$G_{\mathbf{k}}(\tau, \bar{\tau}) = \frac{\sin[k(\tau - \bar{\tau})]}{k}. \quad (76)$$

⁸ Note that we are using the convention at which the spatial part of the metric is given by $a^2(\delta_{ij} + h_{ij}/2)dx^i dx^j$. If we were using an alternative convention $a^2(\delta_{ij} + h_{ij})dx^i dx^j$, then the factor of 1/48 would be replaced by 1/12 as in refs. [58, 59].

⁹ Note that the integration variable u and v are swapped with t and s since in the $t-s$ space, integration limits are independent of the integration variables.

⁷ See also [55–57] for examples where the connected contribution can be important.

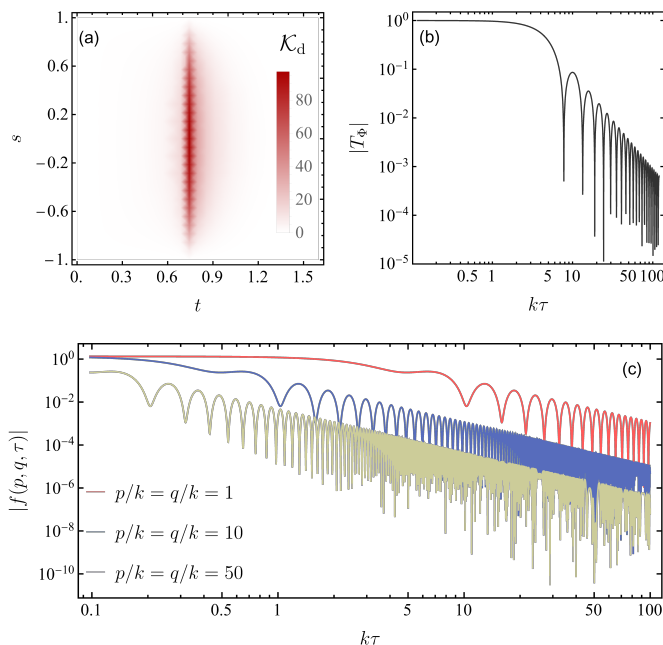


Figure 4. (a) The kernel function from eq. (74). We note a clear resonance contribution from $t \simeq 0.7$ corresponding to $u + v \simeq \sqrt{3}$. (b) The transfer function T_Φ . (c) Function $f(p, q, \tau)$ as in eq. (69). We see that for the scalar modes that enter the horizon earlier, with $p, q > k$, this function is more suppressed as expected from the behavior of the transfer function.

With these expressions, we can obtain a physical understanding of GW generation via eq. (70). The Green function, given in eq. (76), is an oscillatory function of time whose frequency is k . The quantity $f(p, q, \tau)$ is also an oscillatory and decaying function of time (see fig. 4c), inheriting these properties from the transfer function (75). Therefore, the dominant contribution to the integral (68) is a resonant contribution when the momentum of the produced GW is of the same order as the momentum of the scalar modes, i.e., $k \sim p \sim q$. In particular, the resonant point is at $u + v \simeq \sqrt{3}$ [54] as shown in fig. 4a. GW generation is suppressed in other parts of the phase space. For example, the source term, which contains gradients of the curvature perturbation [53], is suppressed by small derivatives if any of the wavenumbers p, q of ζ is much smaller than k . On the other hand, if p, q are much larger than k , then the scalar modes would have decayed significantly after entering the horizon by the time $k \sim H$, and thus the production of GW with momentum k gets suppressed.

To obtain the final result for Ω_{GW} , we note that the GW comoving wavenumber k is related to the present-day, redshifted frequency f of the generated GW via

$$f = f_* \left(\frac{a_*}{a_0} \right) = \frac{k}{2\pi} \simeq 1.5 \text{ mHz} \left(\frac{k}{10^{12} \text{ Mpc}^{-1}} \right), \quad (77)$$

where f_* and a_* are respectively the frequency and the scale factor at the time of GW generation. Using these

expressions, we arrive at our final result, shown in Fig. 5, for the same benchmark choices discussed in Fig. 3. We see that stochastic effects can naturally give rise to a large enough SGWB, within the sensitivity range of DECIGO, BBO, μ -Ares, and Ultimate DECIGO [60–62].

VI. CONCLUSION

In this work, we have discussed an early Universe scenario containing a light spectator field, along with an inflaton field. The fluctuations of the inflaton are red-tilted and explain the observed fluctuations in the CMB and LSS. On the other hand, the spectator field σ naturally acquires a blue-tilted power spectrum. This blue-tilted power spectrum is eventually cut-off at very small scales since when such small-scale modes enter the horizon, the spectator field contributes subdominantly to the total energy density. As a consequence, primordial black holes are not produced in this scenario. Overall, this mechanism of generating a blue-tilted spectrum works for any generic inflaton potential and does not require any particular fine-tuning or structure such as an inflection point or a bump on the potential or an ultra slow-roll phase.

The blue-tilted spectrum gives rise to large curvature perturbations at small scales. These, in turn, source a stochastic gravitational wave background (SGWB) when the perturbations re-enter the horizon. Focusing on some benchmark choices for the number of e -foldings and spectator field potential, we have shown that this scenario predicts observable gravitational waves at future detectors operating in 10^{-5} Hz to 10 Hz range, with strengths $\Omega_{\text{GW}} h^2 \simeq 10^{-20} - 10^{-15}$.

There are various interesting future directions. In particular, we have worked in a regime where σ does not dominate the energy density during the cosmological history. It would be interesting to explore the consequences of an early matter-dominated era caused by the σ field. We have also seen that the low-frequency scaling of the SGWB spectrum depends on the mass and coupling of σ and is generally different from the f^3 -scaling expected in the context of cosmological PT, or $f^{2/3}$ -scaling expected in the context of binary mergers. This different frequency dependence can be used to identify the origin of an SGWB, and distinguish between various cosmological or astrophysical contributions. Along these lines, it would be interesting to carry out a quantitative analysis to understand how well we can separate any two frequency dependencies, for example, by doing a Fisher analysis.

NOTE ADDED

While we were finishing this work, the NANOGrav result combining 15-year data appeared [63]. Secondary gravitational waves from the scalar perturbation can in principle give rise to the signal [64]. Such scalar per-

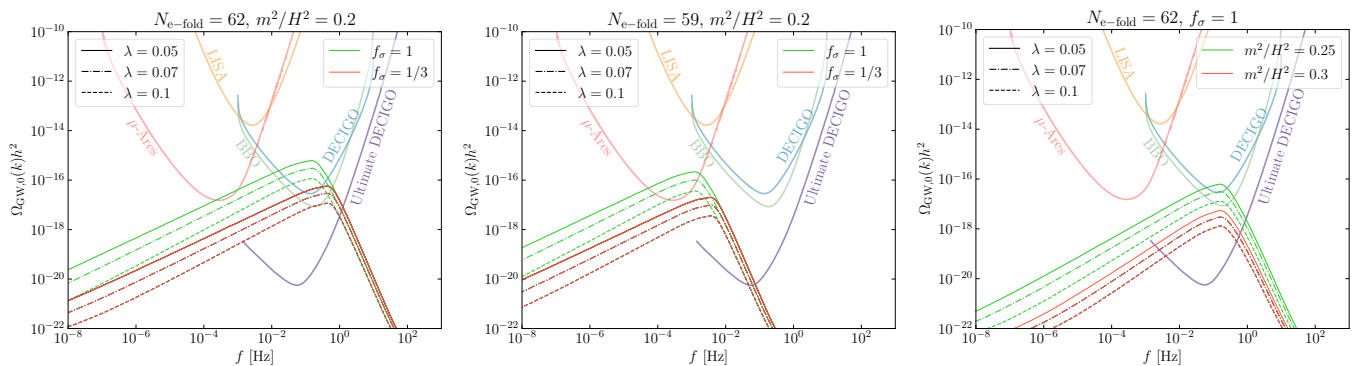


Figure 5. Gravitational wave spectrum for the benchmarks discussed in Fig. 3. We notice that the number of e -folds after CMB-observable modes exited the horizon determines the peak frequency of the spectrum, and correspondingly, different detectors can be sensitive to the signal. Although a similarly peaked spectrum would appear in the context of cosmological phase transitions (PT), the low-frequency tail of this GW spectrum is different from the usual f^3 tail. While in the context of PT the f^3 scaling originates due to causality and superhorizon behavior of fluctuations, in our scenario, the f -scaling is determined by σ mass. The differing frequency dependence can then be used to discriminate between the two classes of signals.

turbations could be generated in a model similar to the one considered in this paper. However, the frequency dependence of $\Omega_{\text{GW}}h^2$ determined by the NANOGrav result is [63] 1.8 ± 0.6 . We note that for a free field with mass m , the frequency dependence of $\Omega_{\text{GW}}h^2$ is given by, $4m^2/(3H^2)$. So for the central value, one would naively infer $m^2/H^2 = 1.4$. Therefore to interpret it in terms of a free field, we require a mass bigger than the Hubble scale. However, since for larger than Hubble-scale masses, the stochastic effects are not efficient, one may have to go beyond the stochastic scenario to explain the NANOGrav observations. We could instead consider a regime in which the misalignment contribution is important [13, 14]. We will leave a detailed analysis of this scenario to future work.

ACKNOWLEDGMENT

We thank Keisuke Harigaya, Andrew Long, and Neal Weiner for their helpful discussions. RE is supported in part by the University of Maryland Quantum Technology Center. SK is supported in part by the National Science Foundation (NSF) grant PHY-1915314 and the U.S. DOE Contract DE-AC02-05CH11231. SK thanks Aspen Center for Physics, supported by NSF grant PHY-2210452, for hospitality while this work was in progress. The research of AM is supported by the U.S. Department of Energy, Office of Science, Office of Workforce Development for Teachers and Scientists, Office of Science Graduate Student Research (SCGSR) program under contract number DE-SC0014664. LTW is supported by the DOE grant DE-SC0013642.

Appendix A: Scalar-induced gravitational waves: technical details

1. Transfer functions

The equation of motion for the scalar perturbation Φ in the absence of isocurvature perturbations is,

$$\Phi''(\tau, \mathbf{k}) + 3(1 + c_s^2)\mathcal{H}\Phi'(\tau, \mathbf{k}) + c_s^2 k^2 \Phi(\tau, \mathbf{k}) = 0, \quad (\text{A1})$$

where $c_s^2 \simeq w$ is the sound speed of the fluid. Defining dimensionless parameter $y = \sqrt{wk}\tau$, we rewrite this equation as

$$\frac{d^2\Phi(y, \mathbf{k})}{dy^2} + \frac{6(1+w)}{1+3w} \frac{1}{y} \frac{d\Phi(y, \mathbf{k})}{dy} + \Phi(y, \mathbf{k}) = 0. \quad (\text{A2})$$

A general solution is given by,

$$\Phi(y, \mathbf{k}) = y^{-\gamma} [C_1(\mathbf{k})J_\gamma(y) + C_2(\mathbf{k})Y_\gamma(y)], \quad (\text{A3})$$

where J_γ and Y_γ are spherical Bessel functions of the first and second kind, respectively, of order γ

$$\gamma = \frac{3(1+w)}{1+3w} - 1. \quad (\text{A4})$$

In the radiation dominated era, in which $w = 1/3 \rightarrow \gamma = 1$, we have

$$\Phi(y, \mathbf{k}) = \frac{1}{y^2} \left[C_1(\mathbf{k}) \left(\frac{\sin y}{y} - \cos y \right) + C_2(\mathbf{k}) \left(\frac{\cos y}{y} + \sin y \right) \right]. \quad (\text{A5})$$

We can deduce the initial conditions of this solution by considering the early-time limit $k\tau \ll 1$,

$$\frac{\sin y}{y} - \cos y \simeq \frac{y^2}{3} \quad \text{and} \quad \frac{\cos y}{y} + \sin y \simeq \frac{1}{y}. \quad (\text{A6})$$

The first term ($\propto C_1$) is then constant in this limit, while the second term ($\propto C_2$) decays as $1/y^3 \sim 1/a^3$. We can therefore assume the initial conditions,

$$C_1(\mathbf{k}) = 2\zeta(\mathbf{k}), \quad C_2(\mathbf{k}) = 0, \quad (\text{A7})$$

which gives a particular solution,

$$\Phi(\tau, \mathbf{k}) = \frac{2}{3}\zeta(\mathbf{k})\frac{3}{y^2}\left(\frac{\sin y}{y} - \cos y\right), \quad (\text{A8})$$

resulting in the transfer function, via (64),

$$T_\Phi(k\tau) = \frac{3}{(k\tau/\sqrt{3})^3}\left(\sin\frac{k\tau}{\sqrt{3}} - \frac{k\tau}{\sqrt{3}}\cos\frac{k\tau}{\sqrt{3}}\right). \quad (\text{A9})$$

We can now see the distinct behavior of super-horizon ($k\tau \ll 1$) and sub-horizon ($k\tau \gg 1$) modes in the radiation dominated era. While the super-horizon modes freeze via our analysis above, the sub-horizon modes oscillate and damp as $\sim \cos k\tau/(k\tau)^2$.

In the matter dominated era, $w = 0$ and the equation of motion for Φ becomes,

$$\Phi''(\tau, \mathbf{k}) + 3\mathcal{H}\Phi'(\tau, \mathbf{k}) = 0, \quad (\text{A10})$$

leading to a constant transfer function.

2. Green's function and GW solution

In this subsection, we discuss in detail the solutions to eq. (60), which is derived using the second-order Einstein equation, $G_{ij}^{(2)} = 8\pi GT_{ij}^{(2)}$, for second-order tensor and first-order scalar contributions. We neglect scalar anisotropic stress, and second-order vector and scalar perturbations. In other words, we use the following perturbed FLRW metric in the Newtonian gauge,

$$ds^2 = -(1 + 2\Phi)dt^2 + a^2\left((1 - 2\Phi)\delta_{ij} + \frac{1}{2}h_{ij}\right)dx^i dx^j, \quad (\text{A11})$$

assuming a perfect fluid energy-momentum tensor with equation of state w . Using lower order solutions and projecting out spatial indices using polarization tensors, i.e. $\epsilon_\lambda^{ij}T_{ij} = T_\lambda$ for any tensor T , we recover (60). For simplicity, we define a new variable $v(\tau, \mathbf{k}) = ah_\lambda(\tau, \mathbf{k})$, which gives the equation of motion for $v(\tau, \mathbf{k})$,

$$v''(\tau, \mathbf{k}) + \left[k^2 - \frac{a''(\tau)}{a(\tau)}\right]v(\tau, \mathbf{k}) = 4a(\tau)\mathcal{S}_\lambda(\tau, \mathbf{k}). \quad (\text{A12})$$

We need the two homogeneous solutions of this equation $v_1(\tau)$ and $v_2(\tau)$ to construct the Green's function,

$$G_{\mathbf{k}}(\tau, \bar{\tau}) = \frac{v_1(\tau)v_2(\bar{\tau}) - v_1(\bar{\tau})v_2(\tau)}{v_1'(\bar{\tau})v_2(\bar{\tau}) - v_1(\bar{\tau})v_2'(\bar{\tau})}. \quad (\text{A13})$$

For each \mathbf{k} we have

$$v_{1,2}''(\tau) + \left[k^2 - \frac{a''(\tau)}{a(\tau)}\right]v_{1,2}(\tau) = 0 \quad (\text{A14})$$

which, using $a \propto \tau^\alpha$ and $x = k\tau$, leads to

$$\frac{d^2v_{1,2}(x)}{dx^2} + \left[1 - \frac{\alpha(\alpha-1)}{x^2}\right]v_{1,2}(x) = 0, \quad (\text{A15})$$

where $\alpha = 2/(1 + 3w)$. The solutions are

$$v_1(x) = \sqrt{x}J_{\alpha-1/2}(x) \quad (\text{A16})$$

$$v_2(x) = \sqrt{x}Y_{\alpha-1/2}(x) \quad (\text{A17})$$

where $J_{\alpha-1/2}$ and $Y_{\alpha-1/2}$ are again spherical Bessel functions of first and second kind, respectively. We note that

$$\frac{dv_1}{dx} = \frac{\alpha}{\sqrt{x}}J_{\alpha-1/2}(x) - \sqrt{x}J_{\alpha+1/2} \quad (\text{A18})$$

$$\frac{dv_2}{dx} = \frac{\alpha}{\sqrt{x}}Y_{\alpha-1/2}(x) - \sqrt{x}Y_{\alpha+1/2}. \quad (\text{A19})$$

Now, we can calculate the expression in the denominator of the Green's function,

$$\begin{aligned} v_1'(x)v_2(x) - v_1(x)v_2'(x) &= kx \left[J_{\alpha-1/2}(x)Y_{\alpha+1/2}(x) - \right. \\ &\quad \left. J_{\alpha+1/2}(x)Y_{\alpha-1/2}(x) \right] \\ &= -\frac{2}{\pi}. \end{aligned} \quad (\text{A20})$$

The second equality can be checked explicitly via `Mathematica`. Thus, (A13) simplifies to

$$\begin{aligned} G_{\mathbf{k}}(\tau, \bar{\tau}) &= \frac{\pi}{2}\sqrt{\tau\bar{\tau}} \left[J_{\alpha-1/2}(k\bar{\tau})Y_{\alpha-1/2}(k\tau) - \right. \\ &\quad \left. J_{\alpha-1/2}(k\tau)Y_{\alpha-1/2}(k\bar{\tau}) \right]. \end{aligned} \quad (\text{A21})$$

In the radiation dominated era, $\alpha = 1$, and so,

$$G_{\mathbf{k}}(\tau, \bar{\tau}) = \frac{\sin k(\tau - \bar{\tau})}{k}, \quad (\text{A22})$$

where we have used (A54) to replace Bessel functions of order 1/2. In the matter dominated era we have $\alpha = 2$, and so,

$$\begin{aligned} G_{\mathbf{k}}(\tau, \bar{\tau}) &= \frac{1}{k} \left[\left(\frac{\bar{\tau} - \tau}{\tau\bar{\tau}}\right) \cos k(\tau - \bar{\tau}) + \right. \\ &\quad \left. \left(\frac{1/k^2 - \tau\bar{\tau}}{\tau\bar{\tau}}\right) \sin k(\tau - \bar{\tau}) \right]. \end{aligned} \quad (\text{A23})$$

where we have again used (A54) to replace Bessel functions of order 3/2.

Having calculated the Green's functions, we can now write the solution for $h_\lambda(\tau, \mathbf{k})$ in the form of (65).

3. Connected and disconnected 4-point correlation function

The primordial 4-point correlation function of ζ can be written in terms of disconnected and connected pieces

$$\begin{aligned} \langle \zeta(\mathbf{k}_1)\zeta(\mathbf{k}_2)\zeta(\mathbf{k}_3)\zeta(\mathbf{k}_4) \rangle &= \langle \zeta(\mathbf{k}_1)\zeta(\mathbf{k}_2)\zeta(\mathbf{k}_3)\zeta(\mathbf{k}_4) \rangle_d \\ &\quad + \langle \zeta(\mathbf{k}_1)\zeta(\mathbf{k}_2)\zeta(\mathbf{k}_3)\zeta(\mathbf{k}_4) \rangle_c, \end{aligned} \quad (\text{A24})$$

where

$$\begin{aligned} \langle \zeta(\mathbf{k}_1)\zeta(\mathbf{k}_2)\zeta(\mathbf{k}_3)\zeta(\mathbf{k}_4) \rangle_d &= \\ (2\pi)^6 \delta^3(\mathbf{k}_1 + \mathbf{k}_2) \delta^3(\mathbf{k}_3 + \mathbf{k}_4) P_\zeta(k_1) P_\zeta(k_3) \\ + (2\pi)^6 \delta^3(\mathbf{k}_1 + \mathbf{k}_3) \delta^3(\mathbf{k}_2 + \mathbf{k}_4) P_\zeta(k_1) P_\zeta(k_2) \\ + (2\pi)^6 \delta^3(\mathbf{k}_1 + \mathbf{k}_4) \delta^3(\mathbf{k}_2 + \mathbf{k}_3) P_\zeta(k_1) P_\zeta(k_4), \end{aligned} \quad (\text{A25})$$

and

$$\begin{aligned} \langle \zeta(\mathbf{k}_1)\zeta(\mathbf{k}_2)\zeta(\mathbf{k}_3)\zeta(\mathbf{k}_4) \rangle_c &= \\ (2\pi)^3 \delta^3(\mathbf{k}_1 + \mathbf{k}_2 + \mathbf{k}_3 + \mathbf{k}_4) \mathcal{T}(\mathbf{k}_1, \mathbf{k}_2, \mathbf{k}_3, \mathbf{k}_4). \end{aligned} \quad (\text{A26})$$

Here, $P_\zeta(k)$ and $\mathcal{T}(\mathbf{k}_1, \mathbf{k}_2, \mathbf{k}_3, \mathbf{k}_4)$ are the scalar power spectrum and trispectrum, respectively. We focus on the disconnected contribution below. The relevant 4-point correlation function for the GW power spectrum (67) is

$$\begin{aligned} \langle \zeta(\mathbf{q}_1)\zeta(\mathbf{k}_1 - \mathbf{q}_1)\zeta(\mathbf{q}_2)\zeta(\mathbf{k}_2 - \mathbf{q}_2) \rangle_d &= \\ (2\pi)^6 \delta^3(\mathbf{k}_1 + \mathbf{k}_2) [\delta^3(\mathbf{q}_1 + \mathbf{q}_2) + \delta^3(\mathbf{k}_1 + \mathbf{q}_2 - \mathbf{q}_1)] \\ \times P_\zeta(q_1) P_\zeta(|\mathbf{k}_1 - \mathbf{q}_1|). \end{aligned} \quad (\text{A27})$$

The two terms in the above expressions are equivalent when substituted in the integrand of (67). The second term can be manipulated as

$$\begin{aligned} \delta^3(\mathbf{k}_1 + \mathbf{k}_2) \delta^3(\mathbf{k}_1 + \mathbf{q}_2 - \mathbf{q}_1) Q_{\lambda_1}(\mathbf{k}_1, \mathbf{q}_1) Q_{\lambda_2}(\mathbf{k}_2, \mathbf{q}_2) \\ \times I(|\mathbf{k}_1 - \mathbf{q}_1|, q_1, \tau) I(|\mathbf{k}_2 - \mathbf{q}_2|, q_2, \tau) \\ = Q_{\lambda_1}(\mathbf{k}_1, \mathbf{q}_1) Q_{\lambda_2}(-\mathbf{k}_1, \mathbf{q}_1 - \mathbf{k}_1) I(|\mathbf{k}_1 - \mathbf{q}_1|, q_1, \tau) \\ \times I(q_1, |\mathbf{k}_1 - \mathbf{q}_1|, \tau) \\ = Q_{\lambda_1}(\mathbf{k}_1, \mathbf{q}_1)^2 I(|\mathbf{k}_1 - \mathbf{q}_1|, q_1, \tau)^2 \end{aligned} \quad (\text{A28})$$

which is the same result we get from the first term. Here we have used identities given in eqs. (A51)-(A53). Thus, the disconnected GW power spectrum is given by (70).

4. Recasting integrals for numerical computation

Here we provide steps to recast (70) into a form suitable for numerical integration.

a. Change of variables. We perform two successive changes of variables to recast the integrals. First, we perform the transformation $\{q, \cos \theta\} \rightarrow \{u, v\}$, where

$$u \equiv \frac{|\mathbf{k} - \mathbf{q}|}{k}, \quad v \equiv \frac{q}{k}, \quad (\text{A29})$$

and the inverse transformation is

$$q = vk, \quad \cos \theta = \frac{1 + v^2 - u^2}{2v}. \quad (\text{A30})$$

The determinant of the Jacobian for this transformation is,

$$\det(J_{\{q, \cos \theta\} \rightarrow \{u, v\}}) = -\partial_v q \partial_u \cos \theta = -\frac{ku}{v}. \quad (\text{A31})$$

which implies

$$\begin{aligned} \int d^3 q &= \int_0^\infty q^2 dq \int_{-1}^1 d \cos \theta \int_0^{2\pi} d\phi \\ &= k^3 \int_0^\infty dv v \int_{|1-v|}^{1+v} du u \int_0^{2\pi} d\phi. \end{aligned} \quad (\text{A32})$$

Second, we perform $\{u, v\} \rightarrow \{s, t\}$ where

$$s \equiv u - v, \quad t \equiv u + v - 1, \quad (\text{A33})$$

and the inverse transformation is

$$u = \frac{s + t + 1}{2}, \quad v = \frac{t - s + 1}{2}. \quad (\text{A34})$$

The determinant of the Jacobian for the second transformation is then

$$\det(J_{\{u, v\} \rightarrow \{s, t\}}) = \frac{1}{2}. \quad (\text{A35})$$

Hence, we have¹⁰

$$\int_0^\infty dv \int_{|1-v|}^{1+v} du = \frac{1}{2} \int_0^\infty dt \int_{-1}^1 ds. \quad (\text{A36})$$

The final result is

$$\int d^3 q = \frac{k^3}{2} \int_0^\infty dt \int_{-1}^1 ds uv \int_0^{2\pi} d\phi. \quad (\text{A37})$$

Above, we express the integrand in terms of u and v for convenience, though the integration itself is done in terms of s and t .

b. Analytic result for the $I(p, q, \tau)$ function. We summarize the results for a radiation-dominated universe (for a more in-depth look, see e.g. [59]). At late times, we have

$$\begin{aligned} I(vk, uk, x/k \rightarrow \infty) &= \frac{1}{k^2} I(u, v, x \rightarrow \infty) \\ &\simeq \frac{1}{k^2} \frac{1}{x} \tilde{I}_A(u, v) \left(\tilde{I}_B(u, v) \sin x + \tilde{I}_C \cos x \right), \end{aligned} \quad (\text{A38})$$

¹⁰ For $v < 1$, the lower limit of integration over s is $1 - 2v$. However, in this case we already have $1 - 2v > -1$.

where we define

$$\tilde{I}_A(u, v) \equiv \frac{3(u^2 + v^2 - 3)}{4u^3v^3} \quad (\text{A39a})$$

$$\tilde{I}_B(u, v) \equiv -4uv + (u^2 + v^2 - 3) \ln \left| \frac{3 - (u + v)^2}{3 - (u - v)^2} \right| \quad (\text{A39b})$$

$$\tilde{I}_C(u, v) \equiv -\pi(u^2 + v^2 - 3)\Theta(u + v - \sqrt{3}). \quad (\text{A39c})$$

In the last expression, Θ is the Heaviside theta function. This result redshifts as $1/x \propto 1/a$. Using the above definitions, we compute the quantity given in A28,

$$\begin{aligned} & \frac{Q_+(\mathbf{k}, \mathbf{q})}{\cos 2\phi} I(|\mathbf{k} - \mathbf{q}|, q, \tau) \\ &= \frac{Q_\times(\mathbf{k}, \mathbf{q})}{\sin 2\phi} I(|\mathbf{k} - \mathbf{q}|, q, \tau) \\ &= \frac{v^2k^2}{\sqrt{2}} \frac{4v^2 - (1 + v^2 - u^2)^2}{4v^2} I(uk, vk, x/k) \\ &\equiv \frac{\tilde{\mathcal{J}}(u, v)}{\sqrt{2}} k^2 I(uk, vk, x/k), \end{aligned} \quad (\text{A40})$$

where we have used dimensionless conformal time $x = k\tau$ and defined

$$\tilde{\mathcal{J}}(u, v) = \frac{4v^2 - (1 + v^2 - u^2)^2}{4}. \quad (\text{A41})$$

When computing the GW power spectrum we are generically interested in the time-averaged quantity

$$\begin{aligned} & \overline{k^2 I(v_1k, u_1k, x/k \rightarrow \infty) k^2 I(v_2k, u_2k, x/k \rightarrow \infty)} = \\ & \frac{1}{2x^2} \tilde{I}_A(u_1, v_1) \tilde{I}_A(u_2, v_2) \\ & \times \left[\tilde{I}_B(u_1, v_1) \tilde{I}_B(u_2, v_2) + \tilde{I}_C(u_1, v_1) \tilde{I}_C(u_2, v_2) \right]. \end{aligned} \quad (\text{A42})$$

c. Azimuthal angle integration. In the disconnected contribution (70), the only ϕ -dependent factors in the integrands are $\sin 2\phi$ and $\cos 2\phi$, coming from Q_λ factors. For each polarization, we then have

$$\int_0^{2\pi} d\phi \sin^2(2\phi) = \int_0^{2\pi} d\phi \cos^2(2\phi) = \pi. \quad (\text{A43})$$

Finally, we are ready to numerically compute the GW energy density (73) which is defined in terms of the dimensionless polarization-averaged GW power spectrum

$$\sum_\lambda \Delta_\lambda^2(\tau, k) = \frac{k^3}{2\pi^2} \sum_\lambda P_\lambda(\tau, k). \quad (\text{A44})$$

Using our recasted variables, the result is

$$\begin{aligned} \Omega_{\text{GW}}(k) \Big|_{\text{d}} &= \frac{2}{48\alpha^2} \left(\frac{k^3}{2\pi^2} \right)^2 \\ & \int_0^\infty dt \int_{-1}^1 ds uv \tilde{\mathcal{J}}(u, v)^2 \tilde{I}_A(u, v)^2 \left[\tilde{I}_B(u, v)^2 \right. \\ & \quad \left. + \tilde{I}_C(u, v)^2 \right] P_\zeta(uk) P_\zeta(vk) \end{aligned} \quad (\text{A45})$$

More compactly,

$$\Omega_{\text{GW}}(k) \Big|_{\text{d}} = \frac{2}{48\alpha^2} \int_0^\infty dt \int_{-1}^1 ds \mathcal{K}_d(u, v) \Delta_\zeta^2(uk) \Delta_\zeta^2(vk) \quad (\text{A46})$$

where we define the following the Kernel functions \mathcal{K}_d for simplified notation,

$$\mathcal{K}_d(u, v) = (uv)^{-2} \tilde{\mathcal{J}}(u, v)^2 \tilde{I}_A(u, v)^2 \left[\tilde{I}_B(u, v)^2 + \tilde{I}_C(u, v)^2 \right]. \quad (\text{A47})$$

5. Useful formula

The projection operator Q_λ (63) is defined as,

$$Q_\lambda(\mathbf{k}, \mathbf{q}) \equiv \epsilon_\lambda^{ij}(\mathbf{k}) q_i q_j = -\epsilon_\lambda^{ij}(\mathbf{k})(\mathbf{k} - \mathbf{q})_i q_j, \quad (\text{A48})$$

where the second equality follows from $\epsilon_\lambda^{ij}(\mathbf{k}) k_i = 0$. If we explicitly set $\hat{k} = \hat{z}$, we have $\mathbf{q} = q(\sin\theta \cos\phi, \sin\theta \sin\phi, \cos\theta)$, where θ and ϕ are polar and azimuthal angles. This leads to the expressions,

$$\begin{aligned} Q_+(\mathbf{k}, \mathbf{q}) &= \frac{q^2}{\sqrt{2}} \sin^2\theta \cos(2\phi), \\ Q_\times(\mathbf{k}, \mathbf{q}) &= \frac{q^2}{\sqrt{2}} \sin^2\theta \sin(2\phi). \end{aligned} \quad (\text{A49})$$

Since $\epsilon_\lambda(\mathbf{k})$ is orthogonal to \mathbf{k} we have

$$Q_\lambda(\mathbf{k}, \mathbf{q}) = Q_\lambda(\mathbf{k}, \mathbf{q} + c\mathbf{k}), \quad (\text{A50})$$

for any constant c . $Q_\lambda(\mathbf{k}, \mathbf{q})$ is also symmetric under $\mathbf{k} \rightarrow -\mathbf{k}$ and $\mathbf{q} \rightarrow -\mathbf{q}$:

$$Q_\lambda(\mathbf{k}, \mathbf{q}) = Q_\lambda(-\mathbf{k}, \mathbf{q}) = Q_\lambda(\mathbf{k}, -\mathbf{q}) = Q_\lambda(-\mathbf{k}, -\mathbf{q}). \quad (\text{A51})$$

Using (69) we see that

$$f(p, q, \tau) = f(q, p, \tau) \quad (\text{A52})$$

and so

$$I(p, q, \tau) = I(q, p, \tau). \quad (\text{A53})$$

a. Bessel functions. The following formulae are helpful for computations involving Bessel functions:

$$\begin{aligned} J_{1/2}(x) &= \sqrt{\frac{2}{\pi x}} \sin x, \\ Y_{1/2}(x) &= -\sqrt{\frac{2}{\pi x}} \cos x, \\ J_{3/2}(x) &= \sqrt{\frac{2}{\pi x}} \left(\frac{\sin x}{x} - \cos x \right), \\ Y_{3/2}(x) &= -\sqrt{\frac{2}{\pi x}} \left(\frac{\cos x}{x} - \sin x \right). \end{aligned} \quad (\text{A54})$$

-
- [1] D. Baumann, “Inflation,” in *Theoretical Advanced Study Institute in Elementary Particle Physics: Physics of the Large and the Small*, pp. 523–686. 2011. [arXiv:0907.5424 \[hep-th\]](#).
- [2] Planck Collaboration, Y. Akrami *et al.*, “Planck 2018 results. X. Constraints on inflation,” *Astron. Astrophys.* **641** (2020) A10, [arXiv:1807.06211 \[astro-ph.CO\]](#).
- [3] K. K. Boddy *et al.*, “Snowmass2021 theory frontier white paper: Astrophysical and cosmological probes of dark matter,” *JHEAp* **35** (2022) 112–138, [arXiv:2203.06380 \[hep-ph\]](#).
- [4] G. Domènech, “Scalar Induced Gravitational Waves Review,” *Universe* **7** no. 11, (2021) 398, [arXiv:2109.01398 \[gr-qc\]](#).
- [5] A. M. Green and B. J. Kavanagh, “Primordial Black Holes as a dark matter candidate,” *J. Phys. G* **48** no. 4, (2021) 043001, [arXiv:2007.10722 \[astro-ph.CO\]](#).
- [6] B. Carr and F. Kuhnel, “Primordial Black Holes as Dark Matter: Recent Developments,” *Ann. Rev. Nucl. Part. Sci.* **70** (2020) 355–394, [arXiv:2006.02838 \[astro-ph.CO\]](#).
- [7] P. Ivanov, P. Naselsky, and I. Novikov, “Inflation and primordial black holes as dark matter,” *Phys. Rev. D* **50** (1994) 7173–7178.
- [8] J. Garcia-Bellido and E. Ruiz Morales, “Primordial black holes from single field models of inflation,” *Phys. Dark Univ.* **18** (2017) 47–54, [arXiv:1702.03901 \[astro-ph.CO\]](#).
- [9] G. Ballesteros and M. Taoso, “Primordial black hole dark matter from single field inflation,” *Phys. Rev. D* **97** no. 2, (2018) 023501, [arXiv:1709.05565 \[hep-ph\]](#).
- [10] N. C. Tsamis and R. P. Woodard, “Improved estimates of cosmological perturbations,” *Phys. Rev. D* **69** (2004) 084005, [arXiv:astro-ph/0307463](#).
- [11] W. H. Kinney, “Horizon crossing and inflation with large eta,” *Phys. Rev. D* **72** (2005) 023515, [arXiv:gr-qc/0503017](#).
- [12] S. Hooshangi, A. Talebian, M. H. Namjoo, and H. Firouzjahi, “Multiple field ultraslow-roll inflation: Primordial black holes from straight bulk and distorted boundary,” *Phys. Rev. D* **105** no. 8, (2022) 083525, [arXiv:2201.07258 \[astro-ph.CO\]](#).
- [13] S. Kasuya and M. Kawasaki, “Axion isocurvature fluctuations with extremely blue spectrum,” *Phys. Rev. D* **80** (2009) 023516, [arXiv:0904.3800 \[astro-ph.CO\]](#).
- [14] M. Kawasaki, N. Kitajima, and T. T. Yanagida, “Primordial black hole formation from an axionlike curvaton model,” *Phys. Rev. D* **87** no. 6, (2013) 063519, [arXiv:1207.2550 \[hep-ph\]](#).
- [15] D. J. H. Chung and H. Yoo, “Elementary Theorems Regarding Blue Isocurvature Perturbations,” *Phys. Rev. D* **91** (2015) 083530, [arXiv:1501.05618 \[astro-ph.CO\]](#).
- [16] D. J. H. Chung and A. Upadhye, “Search for strongly blue axion isocurvature,” *Phys. Rev. D* **98** no. 2, (2018) 023525, [arXiv:1711.06736 \[astro-ph.CO\]](#).
- [17] D. J. H. Chung and S. C. Tadepalli, “Analytic treatment of underdamped axionic blue isocurvature perturbations,” *Phys. Rev. D* **105** no. 12, (2022) 123511, [arXiv:2110.02272 \[astro-ph.CO\]](#).
- [18] A. Talebian, A. Nassiri-Rad, and H. Firouzjahi, “Stochastic effects in axion inflation and primordial black hole formation,” *Phys. Rev. D* **105** no. 10, (2022) 103516, [arXiv:2202.02062 \[astro-ph.CO\]](#).
- [19] P. W. Graham, J. Mardon, and S. Rajendran, “Vector Dark Matter from Inflationary Fluctuations,” *Phys. Rev. D* **93** no. 10, (2016) 103520, [arXiv:1504.02102 \[hep-ph\]](#).
- [20] A. L. Erickcek and K. Sigurdson, “Reheating Effects in the Matter Power Spectrum and Implications for Substructure,” *Phys. Rev. D* **84** (2011) 083503, [arXiv:1106.0536 \[astro-ph.CO\]](#).
- [21] J. Barir, M. Geller, C. Sun, and T. Volansky, “Gravitational Waves from Incomplete Inflationary Phase Transitions,” [arXiv:2203.00693 \[hep-ph\]](#).
- [22] D. J. H. Chung, E. W. Kolb, A. Riotto, and L. Senatore, “Isocurvature constraints on gravitationally produced superheavy dark matter,” *Phys. Rev. D* **72** (2005) 023511, [arXiv:astro-ph/0411468](#).
- [23] A. A. Starobinsky, “STOCHASTIC DE SITTER (INFLATIONARY) STAGE IN THE EARLY UNIVERSE,” *Lect. Notes Phys.* **246** (1986) 107–126.
- [24] A. A. Starobinsky and J. Yokoyama, “Equilibrium state of a selfinteracting scalar field in the De Sitter background,” *Phys. Rev. D* **50** (1994) 6357–6368, [arXiv:astro-ph/9407016](#).
- [25] A. D. Linde and V. F. Mukhanov, “Nongaussian isocurvature perturbations on inflation,” *Phys. Rev. D* **56** (1997) R535–R539, [arXiv:astro-ph/9610219](#).
- [26] K. Enqvist and M. S. Sloth, “Adiabatic CMB perturbations in pre - big bang string cosmology,” *Nucl. Phys. B* **626** (2002) 395–409, [arXiv:hep-ph/0109214](#).
- [27] T. Moroi and T. Takahashi, “Effects of cosmological moduli fields on cosmic microwave background,” *Phys. Lett. B* **522** (2001) 215–221, [arXiv:hep-ph/0110096](#). [Erratum: *Phys.Lett.B* 539, 303–303 (2002)].
- [28] D. H. Lyth and D. Wands, “Generating the curvature perturbation without an inflaton,” *Phys. Lett. B* **524** (2002) 5–14, [arXiv:hep-ph/0110002](#).
- [29] E. W. Kolb and M. S. Turner, *The Early Universe*, vol. 69. 1990.
- [30] K. A. Malik and D. Wands, “Cosmological perturbations,” *Phys. Rept.* **475** (2009) 1–51, [arXiv:0809.4944 \[astro-ph\]](#).
- [31] D. Wands, K. A. Malik, D. H. Lyth, and A. R. Liddle, “A New approach to the evolution of cosmological perturbations on large scales,” *Phys. Rev. D* **62** (2000) 043527, [arXiv:astro-ph/0003278](#).
- [32] M. Sasaki, Y. Nambu, and K.-i. Nakao, “Classical Behavior of a Scalar Field in the Inflationary Universe,” *Nucl. Phys. B* **308** (1988) 868–884.
- [33] Y. Nambu and M. Sasaki, “Stochastic Stage of an Inflationary Universe Model,” *Phys. Lett. B* **205** (1988) 441–446.
- [34] P. W. Graham and A. Scherlis, “Stochastic axion scenario,” *Phys. Rev. D* **98** no. 3, (2018) 035017, [arXiv:1805.07362 \[hep-ph\]](#).
- [35] T. Markkanen, A. Rajantie, S. Stopyra, and T. Tenkanen, “Scalar correlation functions in de Sitter space from the stochastic spectral expansion,” *JCAP* **08** (2019) 001, [arXiv:1904.11917 \[gr-qc\]](#).

- [36] A. R. Liddle and S. M. Leach, “How long before the end of inflation were observable perturbations produced?,” *Phys. Rev. D* **68** (2003) 103503, [arXiv:astro-ph/0305263](#).
- [37] S. Dodelson and L. Hui, “A Horizon ratio bound for inflationary fluctuations,” *Phys. Rev. Lett.* **91** (2003) 131301, [arXiv:astro-ph/0305113](#).
- [38] L. F. Abbott, E. Farhi, and M. B. Wise, “Particle Production in the New Inflationary Cosmology,” *Phys. Lett. B* **117** (1982) 29.
- [39] A. D. Dolgov and A. D. Linde, “Baryon Asymmetry in Inflationary Universe,” *Phys. Lett. B* **116** (1982) 329.
- [40] A. Albrecht, P. J. Steinhardt, M. S. Turner, and F. Wilczek, “Reheating an Inflationary Universe,” *Phys. Rev. Lett.* **48** (1982) 1437.
- [41] D. I. Podolsky, G. N. Felder, L. Kofman, and M. Peloso, “Equation of state and beginning of thermalization after preheating,” *Phys. Rev. D* **73** (2006) 023501, [arXiv:hep-ph/0507096](#).
- [42] J. B. Munoz and M. Kamionkowski, “Equation-of-State Parameter for Reheating,” *Phys. Rev. D* **91** no. 4, (2015) 043521, [arXiv:1412.0656 \[astro-ph.CO\]](#).
- [43] K. D. Lozanov and M. A. Amin, “Equation of State and Duration to Radiation Domination after Inflation,” *Phys. Rev. Lett.* **119** no. 6, (2017) 061301, [arXiv:1608.01213 \[astro-ph.CO\]](#).
- [44] D. Maity and P. Saha, “(P)reheating after minimal Plateau Inflation and constraints from CMB,” *JCAP* **07** (2019) 018, [arXiv:1811.11173 \[astro-ph.CO\]](#).
- [45] S. Antusch, D. G. Figueroa, K. Marschall, and F. Torrenti, “Energy distribution and equation of state of the early Universe: matching the end of inflation and the onset of radiation domination,” *Phys. Lett. B* **811** (2020) 135888, [arXiv:2005.07563 \[astro-ph.CO\]](#).
- [46] R. Allahverdi, R. Brandenberger, F.-Y. Cyr-Racine, and A. Mazumdar, “Reheating in Inflationary Cosmology: Theory and Applications,” *Ann. Rev. Nucl. Part. Sci.* **60** (2010) 27–51, [arXiv:1001.2600 \[hep-th\]](#).
- [47] J. Chluba, R. Khatri, and R. A. Sunyaev, “CMB at 2x2 order: The dissipation of primordial acoustic waves and the observable part of the associated energy release,” *Mon. Not. Roy. Astron. Soc.* **425** (2012) 1129–1169, [arXiv:1202.0057 \[astro-ph.CO\]](#).
- [48] J. Chluba *et al.*, “Spectral Distortions of the CMB as a Probe of Inflation, Recombination, Structure Formation and Particle Physics: Astro2020 Science White Paper,” *Bull. Am. Astron. Soc.* **51** no. 3, (2019) 184, [arXiv:1903.04218 \[astro-ph.CO\]](#).
- [49] V. S. H. Lee, A. Mitridate, T. Trickle, and K. M. Zurek, “Probing Small-Scale Power Spectra with Pulsar Timing Arrays,” *JHEP* **06** (2021) 028, [arXiv:2012.09857 \[astro-ph.CO\]](#).
- [50] K. Van Tilburg, A.-M. Taki, and N. Weiner, “Halometry from Astrometry,” *JCAP* **07** (2018) 041, [arXiv:1804.01991 \[astro-ph.CO\]](#).
- [51] D. J. Fixsen and J. C. Mather, “The Spectral Results of the Far-Infrared Absolute Spectrophotometer Instrument on COBE,” *Astrophys. J.* **581** no. 2, (Dec., 2002) 817–822.
- [52] K. N. Ananda, C. Clarkson, and D. Wands, “The Cosmological gravitational wave background from primordial density perturbations,” *Phys. Rev. D* **75** (2007) 123518, [arXiv:gr-qc/0612013](#).
- [53] D. Baumann, P. J. Steinhardt, K. Takahashi, and K. Ichiki, “Gravitational Wave Spectrum Induced by Primordial Scalar Perturbations,” *Phys. Rev. D* **76** (2007) 084019, [arXiv:hep-th/0703290](#).
- [54] S. Garcia-Saenz, L. Pinol, S. Renaux-Petel, and D. Werth, “No-go theorem for scalar-trispectrum-induced gravitational waves,” *JCAP* **03** (2023) 057, [arXiv:2207.14267 \[astro-ph.CO\]](#).
- [55] P. Adshead, K. D. Lozanov, and Z. J. Weiner, “Non-Gaussianity and the induced gravitational wave background,” *JCAP* **10** (2021) 080, [arXiv:2105.01659 \[astro-ph.CO\]](#).
- [56] C. Unal, “Imprints of Primordial Non-Gaussianity on Gravitational Wave Spectrum,” *Phys. Rev. D* **99** no. 4, (2019) 041301, [arXiv:1811.09151 \[astro-ph.CO\]](#).
- [57] V. Atal and G. Domènech, “Probing non-Gaussianities with the high frequency tail of induced gravitational waves,” *JCAP* **06** (2021) 001, [arXiv:2103.01056 \[astro-ph.CO\]](#).
- [58] M. Maggiore, “Gravitational wave experiments and early universe cosmology,” *Phys. Rept.* **331** (2000) 283–367, [arXiv:gr-qc/9909001](#).
- [59] K. Kohri and T. Terada, “Semianalytic calculation of gravitational wave spectrum nonlinearly induced from primordial curvature perturbations,” *Phys. Rev. D* **97** no. 12, (2018) 123532, [arXiv:1804.08577 \[gr-qc\]](#).
- [60] K. Schmitz, “New Sensitivity Curves for Gravitational-Wave Signals from Cosmological Phase Transitions,” *JHEP* **01** (2021) 097, [arXiv:2002.04615 \[hep-ph\]](#).
- [61] A. Sesana *et al.*, “Unveiling the gravitational universe at μ -Hz frequencies,” *Exper. Astron.* **51** no. 3, (2021) 1333–1383, [arXiv:1908.11391 \[astro-ph.IM\]](#).
- [62] M. Braglia and S. Kuroyanagi, “Probing prerecombination physics by the cross-correlation of stochastic gravitational waves and CMB anisotropies,” *Phys. Rev. D* **104** no. 12, (2021) 123547, [arXiv:2106.03786 \[astro-ph.CO\]](#).
- [63] NANOGrav Collaboration, G. Agazie *et al.*, “The NANOGrav 15 yr Data Set: Evidence for a Gravitational-wave Background,” *Astrophys. J. Lett.* **951** no. 1, (2023) L8, [arXiv:2306.16213 \[astro-ph.HE\]](#).
- [64] NANOGrav Collaboration, A. Afzal *et al.*, “The NANOGrav 15 yr Data Set: Search for Signals from New Physics,” *Astrophys. J. Lett.* **951** no. 1, (2023) L11, [arXiv:2306.16219 \[astro-ph.HE\]](#).